Eur. Phys. J. B **5**, 111–131 (1998)

THE EUROPEAN PHYSICAL JOURNAL B

Collision of a 1–D column of beads with a wall

E. Falcon[a], C. Laroche, S. Fauve, and C. Coste

Laboratoire de Physique, École Normale Supérieure de Lyon, 46 allée d'Italie, 69364 Lyon Cedex 07, France

Received: 6 February 1998 / Revised and accepted: 26 May 1998

Abstract. An experimental study of the collision of a column of N beads ($N \leq 40$) with a fixed wall is presented. For a fixed height of fall and a *rigid wall*, we show that the maximum force felt by the wall is independent of the number of beads N. The duration of impact, the velocity of the deformation wave in the column and an effective restitution coefficient of the column are also measured as a function of N. For a *soft wall*, we show that the maximum force depends on N. A non-dissipative numerical model, based on a nonlinear interaction law between nearest neighbours, gives results in agreement with the experimental data. Moreover, we show that, after the compression phase, the beads of the top of the column separate one after the other from the column with a velocity greater than the initial one. The beads at the bottom then bounce upwards in block, with a velocity smaller than the initial one. We emphasize that this detachment effect results from the energy redistribution within the whole system during the collision and not from any dissipative effect.

PACS. 46.10.+z Mechanics of discrete systems – 83.70.Fn Granular solids – 83.50.Tq Wave propagation, shocks, fracture, and crack healing

1 Introduction

In recent years, the study of granular materials have known a substantial increase of interest (for an overview see Refs. [1,2]). The considered problems mostly deal with the statics (*e.g.*, geometry and compacity of packing, static stresses [3,4]) or the flows (*e.g.*, convection [5,6], fluidization [7–10], surface excitations [11–13]) of granular materials. Other studies tackle an intermediate level and deal with the propagation of deformation in granular media [14–22].

The role of contacts between grains is crucial either to static or dynamic processes. The stresses, in statics, or the compression waves in dynamics transmit only through the network of contacts. In the same way, energy dissipation mostly takes place at the contacts between two grains or between a grain and a wall. In this respect, one–dimensional models may facilitate the understanding of such contact's properties, and are a first step toward more realistic 3–D media. For instance, experimental works have dealt with the propagation of linear or nonlinear waves in a chain of beads [18–21], the behavior of one inelastic ball bouncing repeatedly off the ground [23,24] and the behaviors of one single bead [25,26] or a column of beads [8] undergoing vertical vibrations.

One–dimensional experiments of collision with N bodies ($N \geq 2$) generally lead to surprising results. A single ball, dropped without initial velocity from a height h above a plane, will never bounce back higher than h. But, when a large ball and a small one placed on its top are dropped together, the small ball rebounds much higher than its original height. This effect is known as the *superball effect* [27–30]. In the same way, a horizontal chain of identical beads, each suspended by two threads and initially in contact, exhibits an exotic behavior when a certain number of beads, at one end of the chain, are drawn aside and released. It is a common belief that, after the collision, the same number of beads as the ones initially released, moves away at the far end, the remaining beads being motionless, as a consequence of energy and momentum conservation. But those conservation laws are not sufficient to explain the behavior of a chain of more than 3 beads [31]. Actually, the beads which are generally described as being motionless, are, in fact, separated from their neighbors by a small distance and have some small velocities [32,33].

Theoretical [34] and numerical [35,36] efforts have been made to describe the bounce of inelastically colliding beads on a fixed wall. One of these simulations [35] considers finite duration of a collision and uses *ad hoc* interaction laws whereas the other one [36] is based on series of binary collisions for a column of hard spheres, *i.e.*, for which the collisions are considered as instantaneous. However, until now no experimental work has been done and the behaviors observed numerically rely on unrealistic interaction laws [36] or are without clear interpretation [35].

In this paper, we analyse the dynamics of the collision of a column of N beads with a fixed wall. Initially, the beads are at rest with no separation between them,

[a] e-mail: efalcon@physique.ens-lyon.fr

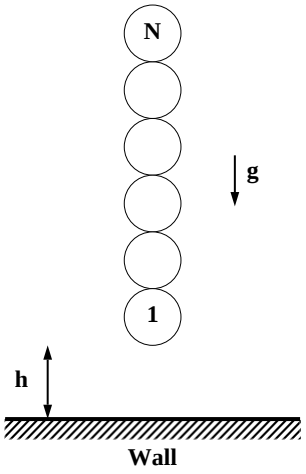

Fig. 1. Problem statement.

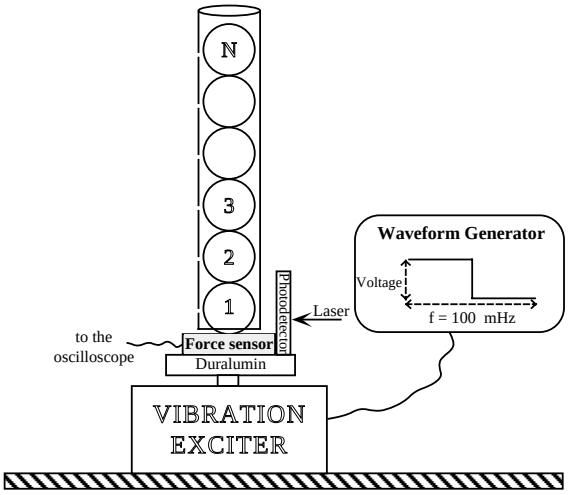

Fig. 2. Schematic diagram of the experimental setup (not to scale).

and they are dropped from a height h above the wall. The problem statement is shown in Figure 1. This system is well adapted to study, in a simple manner, the *detachment effect* observed in 1–D simulations [35] with a linear or nonlinear dissipative interaction law. This effect is discussed in Section 8 while the experimental and numerical observations are presented respectively in Sections 3.5 and 6.6. More generally, the low dimensionality of the experiment and the fact that there is no injected energy during the collision allows a good understanding of elementary mechanisms which play a role in vibrated granular media (see Sect. 9). Finally, this problem raises several questions: how does the force felt by the wall evolve when the number of beads N increases? Do the beads separate from each other after the collision? How does the duration of impact of the whole column scale with N?

This paper is organized as follows. The experimental setup is presented in Section 2. The experimental results are discussed in Section 3. For a fixed height of fall, we show that the maximum force felt by the sensor during the collision of one single bead is exactly the same as for a column of 40 beads! We will see that this astonishing property is linked to the propagation of a deformation wave through the column, and depends on the softness of the wall (see Sect. 4). Moreover, in Section 3, we show that a deformation wave is generated at the beginning of the impact and propagates through the column in the upward direction with a velocity which is an order of magnitude smaller than the speed of sound in the bulk of the bead's material. This velocity is independent of the number of beads. The measurement of the effective restitution coefficient of the column then shows that the greater the number of beads, the greater the energy loss during the collision.

Section 5 is devoted to the presentation of a non–dissipative numerical model. The nonlinear Hertz's law [37] will be used for the description of the interaction between two beads. The outcomes of our numerical work are presented and discussed in Section 6. In Section 7, we derive an expression of the velocity of the deformation wave. Finally, in Section 8, we focus on the mechanism of the bead detachment effect. We emphasize that the detachment effect and also, in a wider sense, the fluidization of vibrated granular systems result from the energy redistribution within the system during the collision, not from any dissipative effect. This redistribution is governed by the intrinsic dispersive nature of compressional wave propagation in the chain. We give our conclusions in Section 9.

2 Experimental setup

A column of N identical stainless steel beads, each one 8 mm in diameter, is put inside a 8.1 mm inner diameter glass tube. The number of beads may vary from $N = 1$ up to $N = 40$. Each bead has a tolerance of $\pm$ 4 μm in diameter and $\pm$ 2 μm in sphericity. The column rests on a PCB 200B02 piezoelectric force sensor screwed on the top of a duralumin cylinder which is itself fixed on an electromagnetic vibration exciter (Brüel and Kjær 4809), as shown in Figure 2. The glass tube is not in contact with the sensor, but is either clamped to a support, 4 mm above the latter, for heights of fall h smaller than the radius R of a bead, or fixed on the duralumin cylinder by means of an angle bar, for $h > R$. The exciter is driven by a square signal of frequency 100 mHz. At first sight, the use of an exciter appears unsuited to free fall experiments. However, as the acceleration of the exciter's table is initially downwards and greater than the acceleration of gravity, the column of beads no more leans on the sensor and starts its free fall. Thus, during one period of the excitation signal and under conditions to be discussed in details in Sections 2.1 and 2.2, the N beads in contact are dropped from a height h above the force sensor. This is possible since the period of the square signal is much greater (10 s) than the time of collision (35 μs for $N = 1$ and 1.04 ms for $N = 40$, both for a height of fall $h = 5.1$ mm). The sensor is connected to a numerical oscilloscope in order to record the collision with the column of beads.

2.1 Reproducibility of the measurements

The reproducibility of the measurements is achieved if all beads are dropped at the same time and are constantly in mutual contact during their free fall. For those reasons, it is necessary to minimize the air friction force on the beads, making holes every 32 mm, along the glass tube, ensuring then the free circulation of air from the inside to the outside of the tube. In order to avoid the beads magnetization caused by the magnetic structure of the exciter, a 5 cm long duralumin cylinder is inserted between the force sensor and the exciter. Moreover, this cylinder absorbs partially the waves generated during the impact, avoiding the reflected waves which could disturb the measurements. In order to check that all beads are constantly in mutual contact during their free fall, a complementary experiment has been done in which the exciter hits the array of beads at rest (see Sect. 3.1). The agreement between both experiments shows that there is no separation between the beads during their free fall (see Sect. 3.1).

2.2 Measurement of the height of fall

The height of fall of the column is of the order of a few millimeters in order to avoid plastic deformation of the sensor. This height is measured by comparing the output signals from the force sensor and from an optical position sensor fixed to the exciter. The position sensor is a photodetector illuminated by a laser diode. The amplitude of the output signal from the position sensor is proportional to the displacement of the exciter's table. Figure 3 shows both output signals from the photodetector (upper curve) and from the force sensor (lower curve) during the fall of 40 beads. It is obvious, from the upper curve in Figure 3, that the shaker does not follow instantaneously the variations of the square signal; its finite response time rather leads to an exponential behavior. The output signal from the force sensor (lower curve in Fig. 3) shows that, during one period of the square signal, the sensor undergoes several collisions. It is clear from this figure that the first collision between the column of beads and the sensor takes place before the exciter's table reaches its minimal position. The height of fall is thus not given by the peak to peak amplitude of the square signal, but by the amplitude A (see Fig. 3) of the output signal from the position sensor. In the case of Figure 3, taking the photodetector sensitivity into account, the value of the height of fall is $h = 5$ mm. The fact that the exciter's table moves downwards during the collision, is not very important since, first, the table velocity during the collision is small compared to the one of the beads, and second, the variation of amplitude ΔA during the collision (see Fig. 3) corresponds to a variation of height Δh smaller than 7×10^{-2} mm, negligible compared to h. This value of Δh has been established in the worst case, *i.e.*, for the greatest collision time observed during our experiments, for a column of 40 beads. With this experimental setup, it is possible to study the collision of N beads with the force sensor for various heights of fall ($1 < h < 5.1$ m) and for $1 < N < 40$.

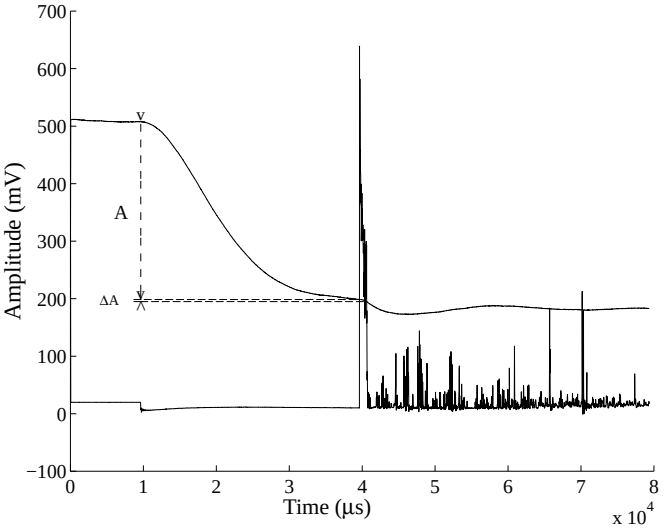

Fig. 3. Output signals from the position sensor (upper curve) and from the force sensor (lower curve) during the fall of $N = 40$ beads. The first peak of the lower curve shows the collision of the column with the sensor whereas the other peaks show the various bounces of the beads. The time scales are the same for both signals, the amplitude scales are different. The upper signal was displaced vertically for clarity. See the text for details.

When the exciter's table starts to move down, the force sensor undergoes a small decompression[1] (see the lower curve of Fig. 3). It means that the column of beads leaves the sensor and starts its free fall. The change in slope observed on the signal of the photodetector, at the end of the collision, reflects the violence of the impact since the motion of the exciter's table is modified by the collision.

3 Experimental results

3.1 Force felt by the force sensor during the collision

The output signal from the force sensor during its collision with a column of N beads is shown in Figure 4 for various values of N and for two different heights of fall. For a fixed height of fall, an astonishing phenomenon occurs. The maximum force F_{max} felt by the force sensor is independent of the number of beads (see Figs. 4a to 4d)! It is also striking that the beginnings of the curves in Figures 4a to 4d are almost superimposed on one another. If we considers only F_{max}, the impact of 1 bead is equivalent to the impact of a column of 40 beads! Paradoxically, we would rather expect that F_{max} is an increasing function of N, for two reasons. Firstly, the greater the number of beads in the column, the greater the impacting mass

[1] This decompression comes from the force variation due to the contact loss, not from the downward acceleration of the sensor. By construction, the dynamical force sensor behaves as an accelerometer when it is loaded, but does not feel any acceleration without load.

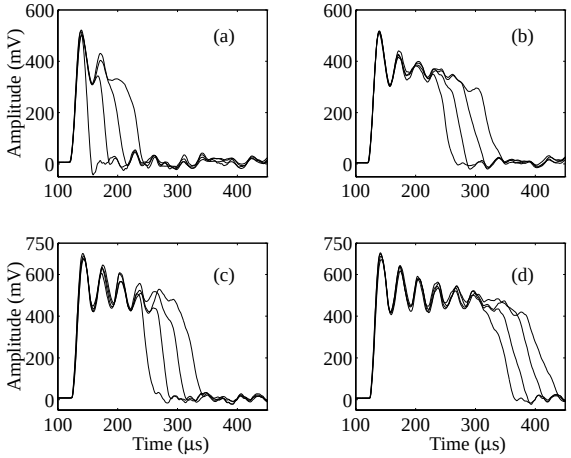

Fig. 4. Output signal from the force sensor during the collision of a column of N beads for two different heights of fall: (a) $N = 1, 2, 3$ or 4 beads with $h = 3.1$ mm; (b) $N = 5, 6, 7$ or 8 beads with $h = 3.1$ mm; (c) $N = 5, 6, 7$ or 8 beads with $h = 5.1$ mm and (d) $N = 9, 10, 11$ or 12 beads with $h = 5.1$ mm. The maximum force F_{max} is 506.7 and 674.5 mV, corresponding to 51.8 and 69 N, for $h = 3.1$ and 5.1 mm respectively.

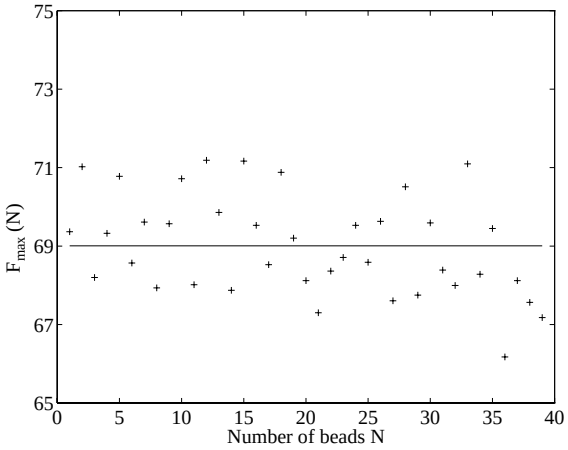

Fig. 5. Maximum force F_{max}, in Newton, as a function of N for $h = 5.1$ mm. Crosses correspond to experimental points and the solid line is the mean value of F_{max} over all measurements.

during the collision. Secondly, Hertz's theory shows that the maximum force during the contact between a sphere of mass m and a plane, scales as $m^{3/5}$. Thus, for a fixed height of fall and for beads with the same radius, the collision of a column of N beads each of mass m is different from the collision of a single bead of mass $M = Nm$:

$$F_{max}(N) \sim N^0 F_{max}(1) \quad \text{for a column of } N \text{ beads of mass } m \text{ each,}$$
$$F_{max}(N) \sim N^{3/5} F_{max}(1) \quad \text{for one bead of mass } M = Nm. \qquad (1)$$

The duration of impact increases linearly with N (see Sect. 3.2). This is consistent since the area under each curve in Figure 4 is the total momentum transfer occurring during the collision, *i.e.*, the product of a force by a time. Thus, as the maximum force is independent of N, the conservation of momentum requires that the duration of impact increases linearly with N. However, as it will be shown later (see Sect. 3.3), the fact that F_{max} is independent of the number of beads is linked to the propagation of a deformation wave in the column generated at the beginning of the impact, and also to the rigidity of the wall. For $h = 5.1$ mm, the experimental values of F_{max} are plotted in Figure 5 as a function of N. F_{max} is actually independent of N since the experimental fluctuations around the mean value $F_{max} = 69$ N appear randomly distributed, lower than 5% of the mean value and of the same order as the fluctuations for different trials with a fixed N. The maximum force is reached after a time interval τ_{max} from the beginning of the impact. τ_{max} is also independent of N (see Fig. 4) and $\tau_{max} = 17.8 \pm 0.5$ μs for $h = 5.1$ mm.

The second interesting phenomenon displayed by all the curves in Figure 4 is the oscillatory nature of the force: the force increases up to F_{max}, then oscillates with a period P before decreasing down to zero. This period is independent of N and seems to depend weakly of the height of fall: $P = 32.4 \pm 1$ μs for $h = 3.1$ mm whereas $P = 31.2 \pm 1$ μs for $h = 5.1$ mm. Moreover, the oscillations are damped around a mean value which seems to decrease very slowly in time (see Fig. 4d). The comparison between the force profile in Figure 4 and the one achieved by non–dissipative numerical simulations (see Fig. 20) shows that this decrease results from the dissipation of energy that occurs during the collision (see Sect. 6.2).

A complementary experiment has been done in order to check that all beads are constantly in mutual contact during their free fall. The force felt by the force sensor should be the same[2] in the case of the free fall of N beads in contact, and in the case of a collision between the sensor and the same chain of beads at rest, *i.e.*, in the reference frame associated to the beads. The experimental setup used to verify this fact is almost identical to the one described in Section 2. The column is now held in a fixed position by means of a diaphragm stuck on the bottom of the glass tube which is clamped to a support. The positive part of the square voltage, generated by the waveform generator, allows then the force sensor to hit the column of beads initially at rest. Figure 6 shows the force profile felt by the force sensor during this collision. The agreement between both experiments (see Fig. 6 and Figs. 4c to 4d) shows that, during their free fall, all beads are constantly in mutual contact. Thus, the force oscillations in Figure 4 are not due to some experimental imperfection leading to a small separation between neighboring beads during their free fall.

3.2 Duration of impact of a column of N beads

The contact time τ_1 between a bead dropped from a height h, and a plane, assumed of infinite mass, is derived from

[2] Before its collision with the chain of beads, no force is exerted on the sensor (see Sect. 2.2).

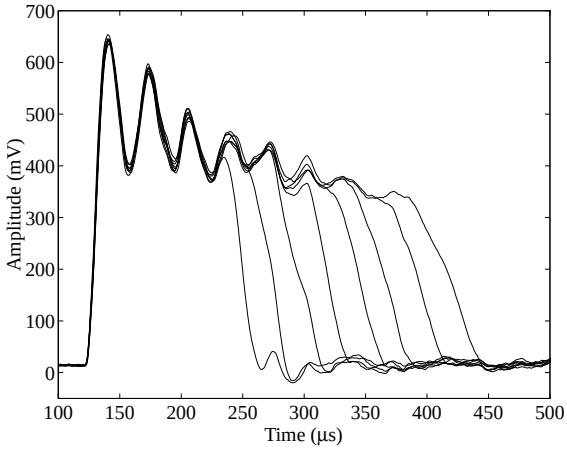

Fig. 6. Output signal from the force sensor during the collision between the sensor and a column of N beads initially at rest when N ranges between 5 and 12.

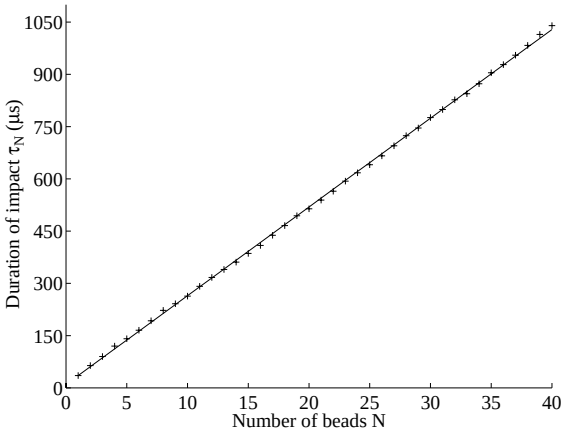

Fig. 7. Duration of impact of a column of N beads, τ_N, as a function of N. The height of fall is $h = 5.1$ mm. Crosses correspond to experimental points and the solid line is the function $\tau_N = (N-1)T_q + \tau_1$ with $T_q = 25.5$ μs and $\tau_1 = 35.5$ μs (see the text for definitions).

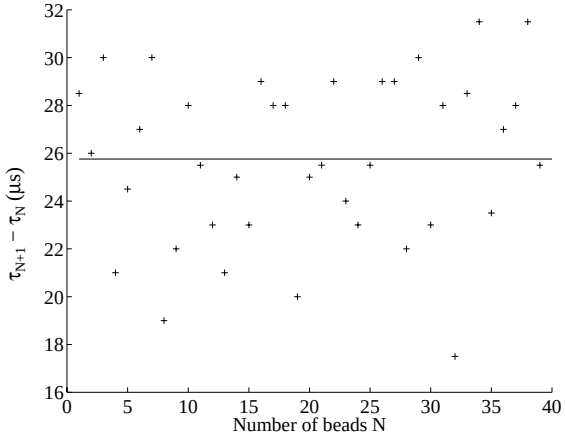

Fig. 8. Evolution of $\Delta\tau_N = \tau_{N+1} - \tau_N$ as a function of N. The height of fall is $h = 5.1$ mm. Crosses correspond to experimental points and the solid line is the mean value of $\Delta\tau_N$ over all measurements: $\langle\Delta\tau_N\rangle = 25.5$ μs.

Hertz's theory [37] and reads

$$\tau_1 = 2.94 \left(\frac{5m}{4K}\right)^{2/5} v_{imp}^{-1/5} , \qquad (2)$$

where m is the mass of the bead, $v_{imp} = \sqrt{2gh}$ its velocity just before the collision, $g = 9.81$ m/s^2 the acceleration of gravity and K the coefficient of the Hertz's interaction for a sphere–plane contact. The value of K depends only on the sphere radius R and on intrinsic characteristics (the Young modulus E_i, the Poisson ratio ν_i) of the sphere ($i = s$) and the plane ($i = p$), and reads

$$K = \frac{4\sqrt{R}}{3} \left(\frac{1-\nu_s^2}{E_s} + \frac{1-\nu_p^2}{E_p}\right)^{-1} . \qquad (3)$$

For a stainless steel bead ($E_s = 21.6 \times 10^{10}$ N/m^2; $\nu_s = 0.276$) with a radius $R = 4$ mm and for a sensor with a stainless steel impact cap ($E_p = E_s$; $\nu_p = \nu_s$), the value of the parameter K is then, from equation (3), $K = 9.858 \times 10^9$ N/m$^{3/2}$.

Let τ_N be the duration of impact (*i.e.*, the contact time) between the column of N beads and the sensor. The measurement of τ_N is extracted[3] from the force profile given by the sensor during the collision. The evolution of τ_N as a function of N, for a height of fall $h = 5.1$ mm, is shown in Figure 7. This latter shows that the duration of impact increases linearly with the number of beads. However, the contact time of a column of N beads is not equal to N times the contact time of one single bead, since the equation of the linear fit displayed in Figure 7 is rather

$$\tau_N = (N-1)T_q + \tau_1 , \qquad (4)$$

where $T_q = 25.5$ μs is the slope of the solid line and $\tau_1 = 35.5$ μs the duration of impact of one single bead.

[3] The value of τ_N is the duration between $F(t = 0)$ and $F(\tau_N) = 0$.

The experimental value τ_1 is in agreement with the theoretical value $\tau_{1_{theo}} = 34.2$ μs coming from equation (2) with $h = 5.1$ mm, $m = 2.05 \times 10^{-3}$ kg and $K = 9.858 \times 10^9$ N/m$^{3/2}$. Besides, as we will see in Section 6.4, the fact that τ_N is not equal to $N\tau_1$ is not due to the fact that during the collision, there are two types of contact (*i.e.*, all of them are between spheres except one, between a plane and a sphere).

Let $\Delta\tau_N$ be the difference between τ_{N+1}, the duration of impact of a column of $N+1$ beads, and τ_N

$$\Delta\tau_N \equiv \tau_{N+1} - \tau_N . \qquad (5)$$

As we can see in Figure 8, within the experimental fluctuations, $\Delta\tau_N$ is independent of N and is equal on average to T_q. Indeed, those fluctuations are of the same order as the ones for different trials with a fixed N. All the dynamics

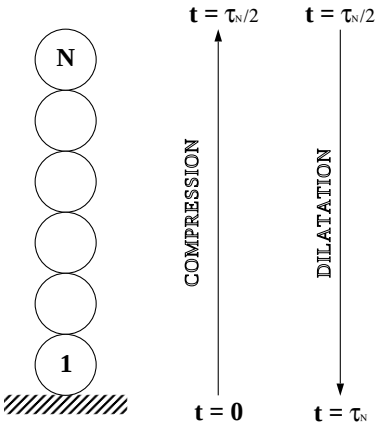

Fig. 9. Direction of propagation of the deformation wave during the collision.

of the collision of N beads seems to be governed by this parameter T_q. Its physical meaning will be explained in Section 3.3.

3.3 Velocity of the deformation wave in the column

During the impact between the column of beads and the sensor, a small part of the incident energy is always lost, in particular into vibrational energy radiated in the sensor from the impact point, in the form of acoustic waves. Those waves, although always present after the initial impact, convert only 1% [38–40] of the incident energy for our range of impact velocities[4]. The greatest fraction of the incident energy is transformed into elastic potential energy stored into the beads during their deformation. This elastic potential energy will be restored during their dilation, corresponding to the bounce of the column. In order to know why and how the column bounces, we must really understand how the presence of the ground disturbs the motion of each bead of the column, *i.e.*, how the deformation, occurring initially between the lower bead and the ground, is transmitted from one bead to another during the collision. Figure 9 shows schematically the direction of propagation of the deformation wave along the column. The initial impact generates a perturbation (compressional wave in the column) which is propagated upwards, then reflected on the top of the column, turned into a dilational wave that propagates downwards. When the wave reaches the bottom of the column, the column leaves the sensor and bounces. Therefore, the duration of impact of the column is the time spent by the wave to travel twice the length of the column. In order to know the velocity of this wave, we have to plot the distance of propagation $4RN$, as a function of the time of propagation τ_N. It is clear from Figure 7 that the velocity of the deformation wave is independent of the number of beads. This velocity is therefore constant along the column. Dividing $4R$ by the slope T_q of the solid line in Figure 7 (see also Eq. (4)) gives the velocity $v = 628$ m/s of the deformation wave in the column for $h = 5.1$ mm. This velocity is an order of magnitude smaller than the speed of sound in a stainless steel rod which is about 5000 m/s. Such a low velocity is also observed in several experiments [18,19,21,32] and simulations [17] dealing with wave propagation in a chain of beads. This results from the discrete nature of the chain which acts like a set of coupled nonlinear oscillators. Indeed, Hertz's works [37] show that, during the compression of a bead, the stress is much greater in the immediate neighborhood of the contact region than throughout the rest of the bead (see also Ref. [41]). The bulk of the bead then acts as an undeformable massive body whereas the material in the neighborhood of the contact region acts as a nonlinear spring.

For identical beads with a radius R, the velocity v of the deformation wave of the column is then given by

$$v = \frac{4R}{T_q} \cdot \tag{6}$$

Consequently, T_q defined as $\langle \Delta T_N \rangle$, represents the time spent by the momentum transfer, from one bead to another, to come and go in one diameter of the bead. This time T_q also corresponds to the time to add to the duration of impact τ_N of a column of N beads in order to obtain the duration of impact τ_{N+1} of a column of $N+1$ beads.

The velocity v of the deformation wave, propagating through the column, was measured experimentally, for various heights of fall h. The results are summarized in Table 1. The velocity increases with the height of fall, *i.e.*, with the impact velocity of the column. As it is shown in Table 1, these results are in fair agreement with the numerical simulations in Section 6.5 and with the analytical expression of the velocity of the deformation wave which is derived in Section 7.

Table 1. Velocity v of the deformation wave for various heights of fall h.

	Velocity v (m/s)		
h (mm)	Experiment	Theory	Simulation
1.9	557	586	583
3.1	586	616	613
5.1	628	647	644

Let us now explain why the maximum force felt by the sensor is independent of the number of beads in the column. As we have seen in Section 3.1, for a height of fall $h = 5.1$ mm and whatever the value of N, the maximum force is reached after a time interval $\tau_{max} = 17.8$ μs from the beginning of the impact. This time is half the collision time $\tau_1 = 35.5$ μs of one single bead for the same height of fall (see Sect. 3.2). Furthermore, for a column

[4] The Reed's theory [40] applied to an impact of a sphere onto a plane both in stainless steel at an impact velocity of 0.3 m/s leads to a dissipated energy in the form of elastic waves equal to 0.65% of the kinetic energy of the bead before the impact.

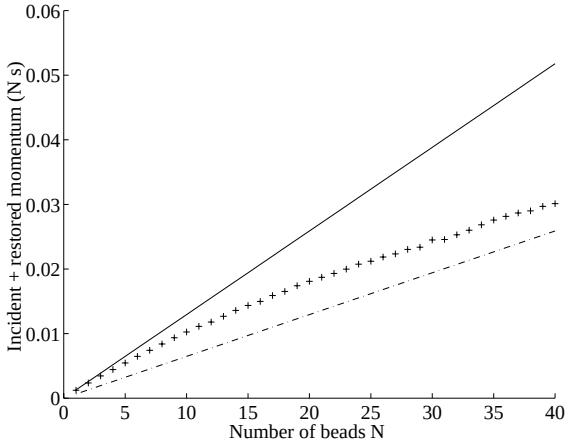

Fig. 10. Sum of the incident and restored momentum as a function of N during the collision of N beads dropped from a height $h = 5.1$ mm. Crosses correspond to experimental points. The solid line corresponds to twice the incident momentum $2mv_{imp}N$, which should be conserved during the collision, if the impact were perfectly elastic. The dot–dashed line corresponds to $mv_{imp}N$, the case where the collision should be perfectly inelastic.

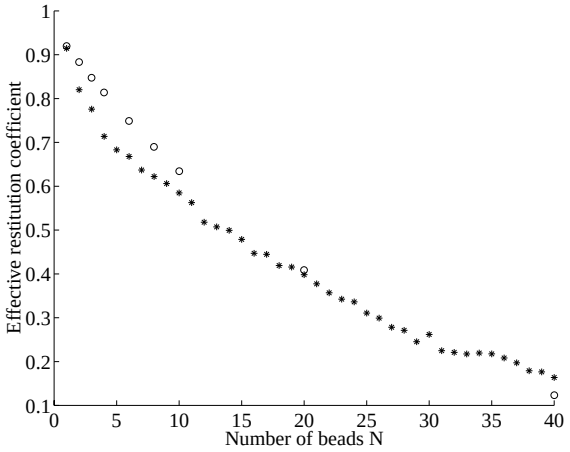

Fig. 11. Restitution coefficient of the whole column (see Eq. (7)) as a function of N during the collision of N beads dropped from a height $h = 5.1$ mm. Crosses correspond to experimental points. Circles correspond to event–driven simulations of Luding [42] for initial velocities $v_{imp} = 0.31$ m/s of each particle, the particle–particle coefficient of restitution and the particle–wall one being respectively 0.96 and 0.92.

of N beads, the sensor feels the presence of the second bead when the deformation wave reaches the second bead and returns to the sensor, *i.e.*, after a time $T_q = 25.5$ μs from the beginning of the impact. Consequently, the sensor feels only one bead for times $0 < t < T_q$, whatever the number of beads in the column. Since the maximum of the loading cycle of this bead is reached at τ_{max} and since $\tau_{max} < T_q$, the maximum force is therefore independent of the number of beads in the column. This behavior corresponds to the case of a collision with a *rigid wall*. Hereafter, a collision with a *rigid wall* will be defined as a collision such that $\tau_{max}(N = 1) < T_q$ whereas a collision with a *soft wall* will correspond to the opposite inequality, *i.e.*, $\tau_{max}(N = 1) \geq T_q$. As it will be shown experimentally in Section 4 and numerically in Section 6.7, in the case of a collision with a *soft wall*, the maximum force depends on N.

3.4 Effective restitution coefficient

The total momentum transfered during the collision of a column of N beads with the sensor is given by the area under the curve displaying the temporal evolution of the force. Indeed, in the ideal case of a dissipationless elastic collision, the area under the curve corresponds to the sum of the incident momentum (loading cycle) and the restored momentum (unloading cycle), *i.e.*, twice the incident momentum. In the case of an inelastic collision, a part of the incident energy is dissipated and the area under the curve is therefore smaller. Figure 10 shows that the collision of N beads dissipates more and more energy as N increases. This explains why the mean value of the force in the oscillatory regime decreases slowly in time (see Fig. 4d).

For a collision between one bead and a plane at rest, the coefficient of restitution is usually defined as the ratio of the bead's velocity after and before the collision. For N beads, we introduce the effective restitution coefficient of the whole column

$$\epsilon_{eff} \equiv -\frac{\sum_{i=1}^{N} v_i^{\mathrm{f}}}{\sum_{i=1}^{N} v_i^{\mathrm{i}}} = -\frac{1}{N v_{imp}} \sum_{i=1}^{N} v_i^{\mathrm{f}} \ , \qquad (7)$$

where v_i^{f} and v_i^{i} denotes the velocity of the i-th bead respectively after and before the collision. This definition of ϵ_{eff} is choose because experimentally we only have access to the total momentum of the system. When $N = 1$, equation (7) is identical to the usual definition of the restitution coefficient. In Figure 11 we display ϵ_{eff} as a function of N. Those experimental values of ϵ_{eff} are extracted, for each N, from the total momentum of the column (see crosses in Fig. 10) and the incident momentum Nmv_{imp}. We find that ϵ_{eff} decreases with N, in our range of N. This means that the momentum loss of the column of N beads during the collision increases with increasing N. Using equation (7) as the definition of the effective restitution coefficient, Luding [42] shows in event–driven simulations, that ϵ_{eff} decreases with N (see ($\circ$) symbols in Fig. 11). We can extend this result for the momentum loss to the energy loss. However, using molecular–dynamics simulations, Luding *et al.* [35] show with a linear dissipative interaction law, that the energy loss decreases with increasing N and is almost independent of N, with a nonlinear dissipative interaction. This apparent discrepancy may be due to the fact that these authors use a different definition for the effective coefficient of restitution of the whole column (see Eq. (30) in Sect. 8 and also Ref. [35]) or

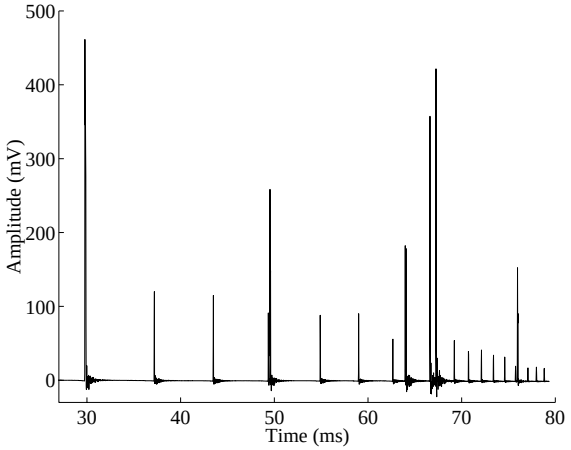

Fig. 12. Example of temporal evolution of the output signal from the force sensor for $N = 5$ and $h = 2.7$ mm. The first peak is the first collision between the whole column and the sensor. The other peaks are the various bounces of beads. The sensitivity of the oscilloscope is 7 μs/pt ; 80 000 points have been recorded and each peak is made of 7 points at least.

to the fact that molecular dynamics or event-driven methods lead to completely different evolutions of the effective restitution coefficient as a function of N [45].

3.5 Detachment of the beads from the column

In order to know how the column of beads bounces after the collision, we have to record the output signal from the force sensor over a time much longer than the duration of impact of the column. Figure 12 shows the temporal evolution of such a signal. The first peak, on the left side in Figure 12, corresponds to the first collision of the whole column with the sensor. The other peaks are the various bounces of beads. Figure 12 shows that the column does not bounce as a whole. In that case, the dissipation would impose a slow monotonous decrease of the peak amplitudes. The appearance of peaks with high amplitude among the peaks with decreasing amplitude proves the opposite. Therefore, the beads are no longer in contact after the collision between the column and the sensor. This detachment of the beads is consistent with the one found numerically in Sections 6.1 and 6.6, and is discussed in detail in Section 8.

4 Collision with a soft wall

Let us now consider the collision of a column of N beads with a soft wall. Both definitions of a soft wall and a rigid wall have been given in Section 3.3. The experimental setup is as in Section 2 except that the force sensor is covered with a sheet either in brass, adhesive tape, PVC, PMMA, cardboard, rubber or beech. Two different sorts of cardboard are used and are called afterwards cardboard I and cardboard II. The thickness of each material sheet is about 1 mm (see Tab. 2). For all experiments discussed in this section, the value of the height of fall is $h = 2.9$ mm. Consequently, the impact velocity of the column is fixed whatever the choice of the material sheet stuck on the sensor.

Table 2. Experimental results during the collision between N stainless steel beads and a force sensor covered with various material sheets, for a fixed height of fall $h = 2.9$ mm.

Material	Thickness (mm)	N_d	$\tau_{max}(N=1)$ (μs)	$\tau_{max}(N=N_d)$ (μs)
none	-	1	17	17
brass	1.2	2	47.5	46
adhesive tape	0.3	4	47.5	112
PVC	1	6 ± 1	67.5	171 ± 19
PMMA	1	8 ± 1	69	228 ± 11
cardboard II	0.5	11 ± 1	191	396 ± 21
beech	2	15 ± 1	127.5	468 ± 26
cardboard I	0.8	22 ± 2	227	743 ± 23
rubber	1	28 ± 4	221	950 ± 57

The output signal from the force sensor during the collision of the column of N beads is shown in Figure 13 for different values of N and for various material sheets stuck on the sensor. Except for Figure 13a, the maximum force felt by the sensor now depends on the number of beads (see Figs. 13b to 13f). The maximum force increases with N at low values of N, until it becomes independent of N. When the sensor is not covered with any material sheet (see Fig. 13a), the experimental results are the same as the ones in Section 3: Independence of the maximum force felt by the sensor as N increases and oscillatory nature of the force. Notice that this latter property is never observed when a soft material sheet is stuck on the sensor. For each material, the experimental values of F_{max} are plotted in Figure 14 as a function of N. For a given material, let us denote N_d the critical number of beads above which F_{max} becomes independent of N. It is clear from Figure 14 that as the material becomes softer, the critical number of bead N_d increases. For each material, the difference $\Delta\tau_N$ between τ_{N+1}, the duration of impact of a column of $N+1$ beads, and τ_N is shown in Figure 15 as a function of N. Figure 15a shows that within the experimental errors, $\Delta\tau_N$ is independent of N and of the material sheet stuck on the sensor. This is in agreement with the experimental results in Section 3.2 and the interpretation of $\Delta\tau_N$ given in Section 3.3: $\Delta\tau_N$ is equal on average to T_q which depends only on the contact between adjacent beads. The experimental value of $T_q = \langle\Delta\tau_N\rangle = 28.6$ μs is then extracted from Figure 15a. However, for the softer materials, at low values of N, $\Delta\tau_N$ is both dependent of N and of the nature of the material stuck on the sensor (see Fig. 15b), this boundary effect vanishing at higher values of N.

Let us now explain why, according to the rigidity of the wall, the maximum force felt by the sensor is either dependent or independent of the beads number in the column.

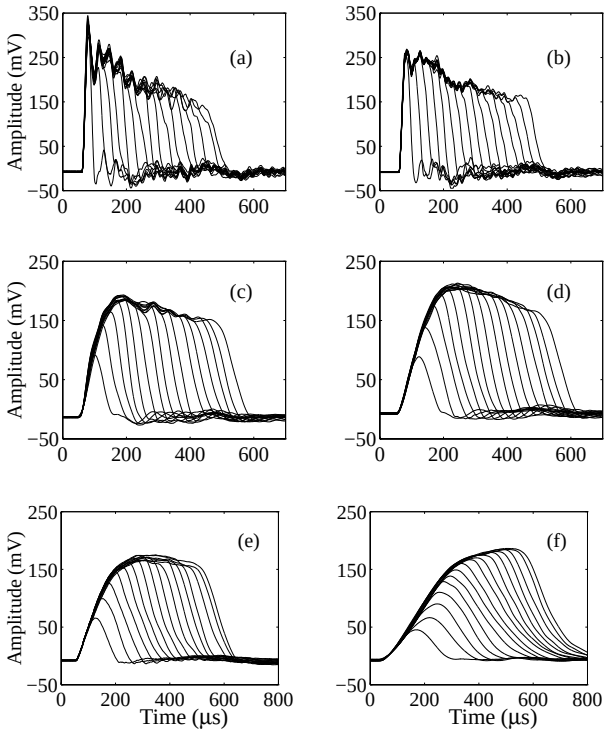

Fig. 13. Output signal from the force sensor during the collision of a column of N beads for different material sheets stuck on the sensor: (a) none; (b) brass; (c) adhesive tape; (d) PVC; (e) PMMA; (f) beech. In all cases, N varies from 1 to 16 and $h = 2.9$ mm.

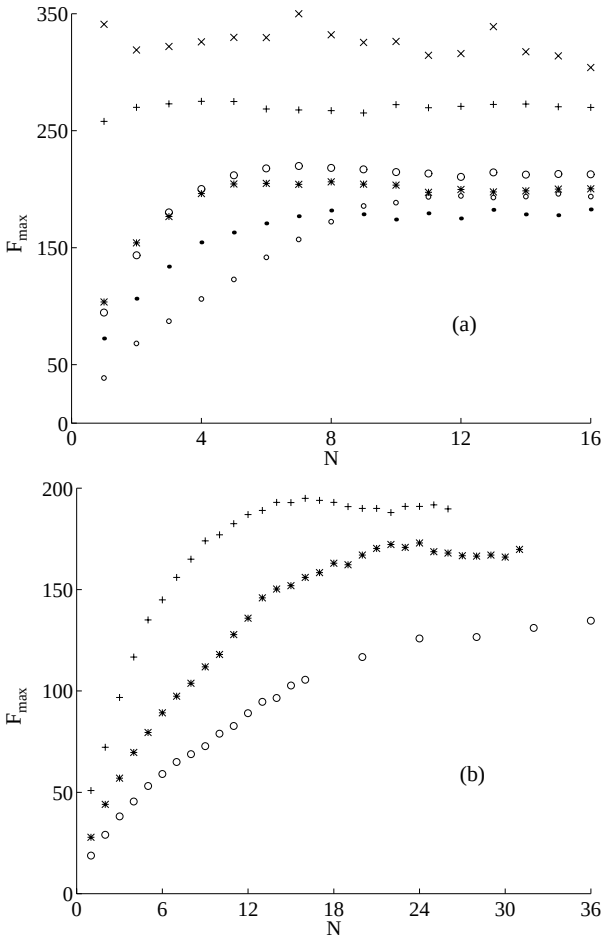

Fig. 14. Maximum force F_{max}, in Newton, as a function of N for $h = 2.9$ mm for different material sheets stuck on the sensor: (a) ($\times$) none; ($+$) brass; ($*$) adhesive tape; ($\circ$) PVC; ($\bullet$) PMMA; ($\circ$) cardboard II. (b) ($+$) beech; ($*$) cardboard I; ($\circ$) rubber.

For a column of N beads, the maximum force $F_{max}(N)$ is reached after a time interval $\tau_{max}(N)$ from the beginning of the impact and is independent of the number of beads for $N \geq N_d$. As we have seen in Section 3.3 for a rigid wall, the independence of F_{max} from N is linked to the propagation of the deformation wave through the column and is due to the fact that $\tau_{max}(N = 1) < T_q$, τ_{max} being in this case independent of N since $N_d = 1$. In the case where $\tau_{max}(N = 1) \geq T_q$, the sensor feels the presence of several beads before the first bead reaches the maximum of its loading cycle. Consequently, the maximum force $F_{max}(N)$ increases with N. The critical number of beads N_d above which the maximum force becomes independent of N is then reached since the deformation wave propagated through a distance $4RN_d$ during a time $\tau_{max}(N_d)$. The velocity of the deformation wave being given by equation (6), the critical number of bead N_d reads

$$N_d = \left\lceil \frac{\tau_{max}(N_d)}{T_q} \right\rceil , \qquad (8)$$

where $\lceil x \rceil$ is the least integer not smaller than x.

Experimentally, for each material sheet stuck on the sensor, the value of N_d is extracted from Figure 14 and the values of $\tau_{max}(N = 1)$ and $\tau_{max}(N = N_d)$ are measured from the temporal evolution of the maximum force. Those results are summarized in Table 2. The above interpretation is in agreement with these results since when $\tau_{max}(N = 1) < T_q$ (resp. $\geq T_q$), $N_d = 1$ (resp. $N_d > 1$). N_d is plotted in Figure 16 as a function of $\tau_{max}(N_d)$. Each cross corresponds to a set of experiments for one given material. The solid line corresponds to the value of N_d extracted from equation (8) with $T_q = 28.6$ μs. The agreement between the experimental data and the prediction is very good except for the softer materials (rubber, beech, cardboard I and II). The reason is that, for each of these materials, the value of $\Delta\tau_N$ is not independent of N (see Fig. 15b) and consequently T_q is not defined. This means that the emission of the deformation wave is strongly modified by the presence of a very soft impact pad. Indeed, instead of creating a deformation wave with a steep front, as it is assumed in Section 7, such an impact generates a wave with a smoothed–out step front. As the chain of beads is a dispersive medium (see Sect. 8), the velocity of such waves then may be considerably modified. Finally, in Section 6.7, we will see that the numerical results are consistent with these experimental results.

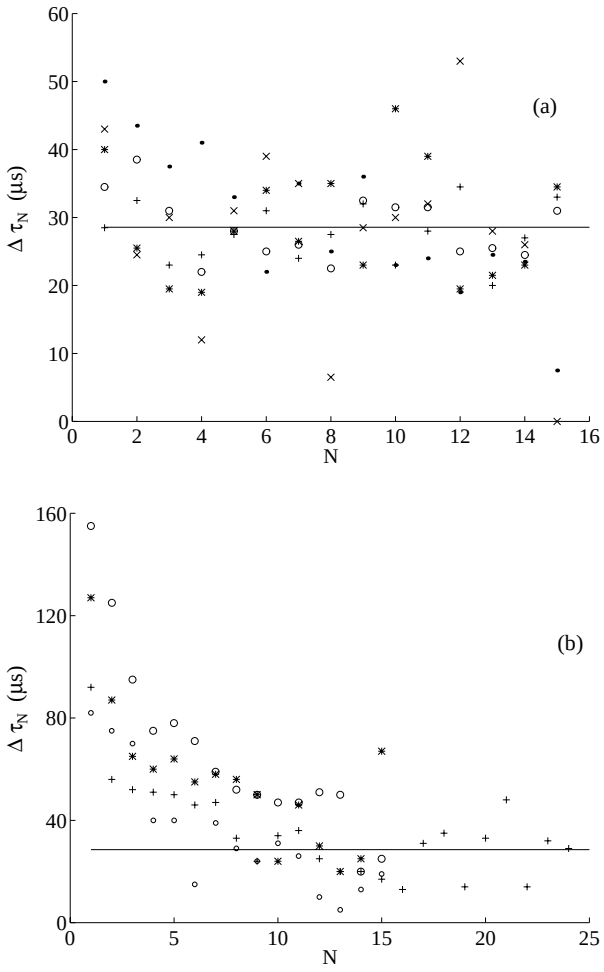

Fig. 15. Evolution of $\Delta\tau_N = \tau_{N+1} - \tau_N$ as a function of N for different material sheets stuck on the sensor: (a) ($\times$) none; ($+$) brass; ($*$) adhesive tape; ($\circ$) PVC; ($\bullet$) PMMA. (b) ($\circ$) rubber; ($+$) beech; ($*$) cardboard I; ($\circ$) cardboard II. In all cases, the height of fall is $h = 2.9$ mm. The solid line is the mean value of $\Delta\tau_N$ over all measurements in figure (a): $\langle\Delta\tau_N\rangle = 28.6$ μs.

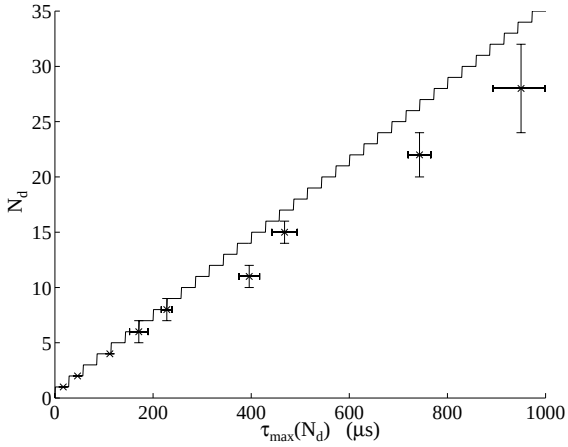

Fig. 16. Evolution of N_d as a function of $\tau_{max}(N_d)$. Each cross corresponds to each set of experiments made with one given material (see data in Tab. 2). Solid line corresponds to the values of N_d deduced from equation (8) with $T_q = 28.6$ μs.

5 Non–dissipative numerical model

Our purpose in this section is to present a simple numerical model which reproduces the experimental results reported in Section 3 for a rigid wall: independence of the maximum force felt by the sensor as N increases (Sect. 3.1), velocity of the deformation wave (Sect. 3.3), bead detachment effect from the column (Sect. 3.5) and the ones in Section 4 for a soft wall: dependence of the maximum force on N.

In this model, we neglect all dissipative mechanisms. Moreover, as we have demonstrated experimentally in a recent study [23], we can disregard the gravity force with respect to the elastic force, during the interaction, for heights of fall of the order of magnitude of the millimeter. Thus, in the following model, only the Hertz's law of contact will be taken into account. All the typical times in the problem are greater than the travel time of a bulk acoustic wave across the bead. For a stainless steel sphere with radius $R = 4$ mm, the period associated with the lowest eigenfrequency of radial vibrations of the elastic sphere is 2 μs [37]. The smallest time in the problem is the duration of collision of one single bead which is experimentally 35.5 μs for the maximum height of fall $h = 5.1$ mm. Consequently, the column can be treated as a chain of N mass points of mass m, each one interacting with its nearest neighbors through the Hertz's law, *i.e.*,

$$F_i = \begin{cases} k(x_{i+1} - x_i)^{3/2} \text{ if } x_{i+1} - x_i > 0 \\ 0 \qquad\qquad\quad \text{otherwise} \end{cases}$$
$$\forall\ 1 \leq i \leq N-1\ , \tag{9}$$

where F_i is the interaction force between the ith and the $i+1$th mass, x_i the displacement of the ith masspoint from its initial position x_{0_i} without deformation, and k is a constant given in equation (12). With the convention on the positive direction of displacements x_i (see Fig. 17), the ith mass interacts with the $i+1$th, through the Hertz's law, if $x_{i+1} - x_i > 0$ (see Fig. 17b) whereas they separate from each other if $x_{i+1} - x_i < 0$.

At $t = 0$ (see Fig. 17a), all the nonlinear springs are uncompressed, and an identical velocity v_{imp} is imposed to each bead. The initial conditions of the problem are thus

$$\begin{cases} x_i(t=0) = 0 \\ \dot{x}_i(t=0) = v_{imp} \end{cases} \qquad \forall\ 1 \leq i \leq N\ . \tag{10}$$

The sensor is represented by a nonlinear spring of constant K linked to an infinite mass. The parameter K of this spring is different from k, proper to all the other springs, in order to be close to the experimental conditions, since the Hertz's law coefficient for a sphere–plane contact is different from the one for a sphere–sphere contact.

With this supplementary condition and the interaction forces given by equation (9), the system is described by

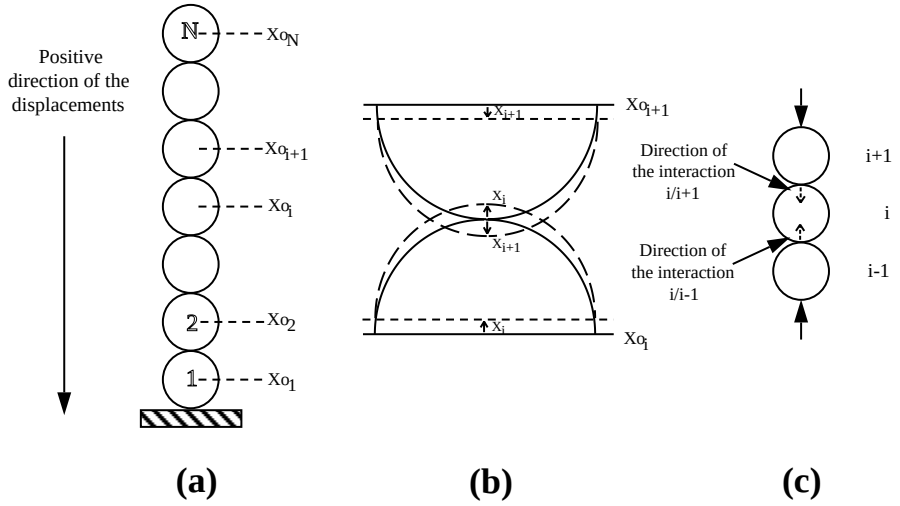

Fig. 17. Schematic diagram of the numerical model: (a) initial conditions: all masses i are in their initial position x_{0_i} without deformation; (b) interaction between the ith and the $i+1$th bead: $x_{i+1} - x_i > 0$ corresponds to an *interpenetration* between the two beads (or a compression of the nonlinear spring) whereas $x_{i+1} - x_i < 0$ means that the beads are no more in contact (or the two springs are separated from each other); (c) directions of the interactions between the ith and the $i+1$th bead and between the $i-1$th and the ith bead.

the following set of N coupled differential equations

$$\forall t \neq 0,\ \begin{cases} m\ddot{x}_N = -F_{N-1}\ , \\ m\ddot{x}_i = F_i - F_{i-1} \text{ for } 2 \leq i \leq N-1\ , \\ m\ddot{x}_1 = F_1 - F_0 \quad \text{where } F_0 = \begin{cases} K x_1^{3/2} & \text{if } x_1 > 0\ , \\ 0 & \text{otherwise.} \end{cases} \end{cases} \tag{11}$$

A fourth order Runge–Kutta method is used for numerically solving the system of nonlinear equations (11). During the calculation the total energy is conserved with an accurary better than 10^{-4} %. The integration time step used is much lower than the typical impact time[5] of two spheres: the impact time is about 40 μs and the time step 0.25 μs.

The force felt by *the sensor* is $Kx_1^{3/2}(t)$ where K is the coefficient of the Hertz's law for a sphere–plane contact (see Eq. (3)). The value of parameter k is derived from the Hertz's law for a sphere–sphere contact. It depends only on the sphere radius R and on intrinsic characteristics (the Young modulus E_s, the Poisson ratio ν_s) of the sphere material, and reads

$$k = \frac{\sqrt{2R}}{3} \frac{E_s}{1-\nu_s^2}\ \cdot \tag{12}$$

In order to compare quantitatively the experimental results for a rigid wall with those of the simulations, k is calculated for a contact between two stainless steel spheres ($E_s = 21.6 \times 10^{10}$ N/m^2, $\nu_s = 0.276$), of radius $R = 4$ mm. K is calculated for a contact between a sphere and a plane both in stainless steel. Thus, from equations (3) and (12), $k = 6.9716 \times 10^9$ N/m$^{3/2}$ and $K = 9.858 \times 10^9$ N/m$^{3/2}$. For most simulations, the choice for the impact velocity of the column, $v_{imp} = 0.3$ m/s, will correspond to a height of fall of 4.6 mm.

[5] This impact time is the smallest time scale appearing in the system, since equations (11) are defined in the quasi–static limit where acoustic wave propagation within a bead is neglected.

6 Numerical results

6.1 Displacement and velocity of each bead during the collision

Figure 18 shows the temporal evolution of displacements $x_i(t)$, compared to their initial position, of each bead i during the collision of a column of $N = 7$ beads with a wall. With the conventions in Figure 17, a compression of the ith bead corresponds to a positive displacement x_i. The seventh bead (*i.e.*, the one at the top of the column) embeds itself linearly during the loading cycle (x_7 increases), then performs its unloading cycle (x_7 decreases), before separating from the sixth bead ($x_7 - x_6 < 0$) and going away upwards indefinitely with a constant velocity since the gravity is neglected. The bead at the bottom of the column (bead 1) embeds itself, then oscillates around a constant displacement, during all the collision, before doing its unloading cycle and leaving the wall ($x_1 < 0$). When the bead 1 has finished its loading cycle ($t = 16$ μs), it has stored elastic energy which allows it to start its unloading cycle before the bead 2 forces it to embed itself once again since the loading elastic energy stored by bead 2 is greater than the unloading elastic energy stored by bead 1. The beads i, with $i \geq 2$, have an influence on the motion of the bead 1 and this seems to be the reason for the oscillations of the displacement x_1. As shown in Figure 18, the seventh bead separates from the sixth ($x_7 - x_6 < 0$) while the other beads are still in interaction, then the sixth separates from the fifth ($x_6 - x_5 < 0$), *etc.* Therefore, the

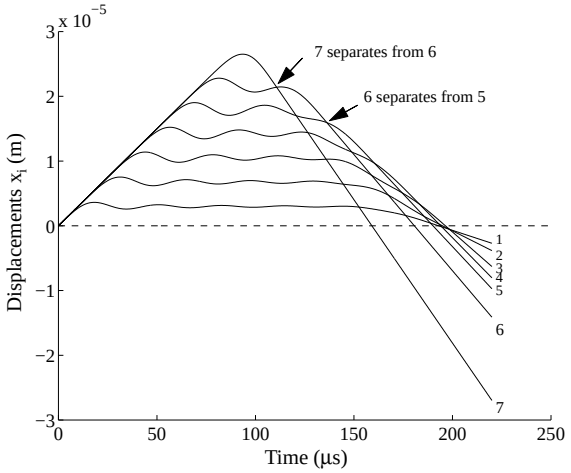

Fig. 18. Result of numerical simulations: temporal evolution of displacements $x_i(t)$ from their initial positions x_{0_i}, of each bead i during the collision of a column of $N = 7$ beads with a wall. This displacement $x_i(t)$ becomes positive since the ith bead is compressed. The dashed line corresponds to the zero deformation, *i.e.*, when all the beads are in their initial position. From this dashed line, the successive solid lines correspond respectively to the displacements $x_i(t)$ from $i = 1$ to 7. The simulation has been done for $v_{imp} = 0.3$ m/s; $m = 2.05 \times 10^{-3}$ kg; $k = 6.9716 \times 10^9$ N/m$^{3/2}$ and $K = 9.858 \times 10^9$ N/m$^{3/2}$ and has been stopped at $T = 220$ μs.

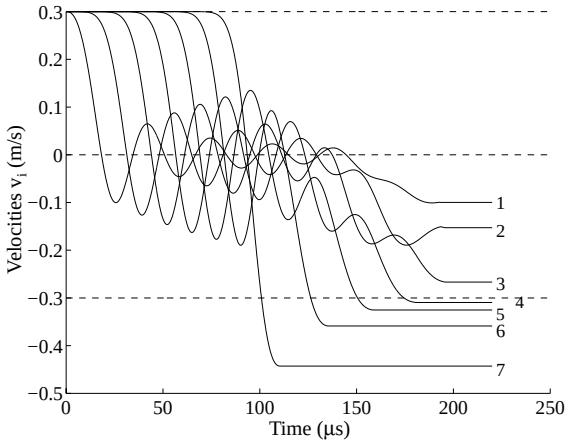

Fig. 19. Result of numerical simulations: temporal evolution of velocities $\dot{x}_i(t)$ of each bead i during the collision of a column of $N = 7$ beads with a wall, for $v_{imp} = 0.3$ m/s. The dashed line at -0.3 m/s corresponds to the limit beyond which the beads 1 to 3 separate from the column with a velocity smaller than their initial one v_{imp}. Below this limit, the beads 4 to 7 separate from the column with a velocity greater than v_{imp}. The parameters of the simulation are as in Figure 18.

beads of the top of the column seem to separate one after the other before the end of the collision.

Figure 19 shows the evolution of the velocities $\dot{x}_i(t)$ of each bead i for $N = 7$ and $v_{imp} = 0.3$ m/s. During the collision, the permanent exchange of momentum between all beads generates the velocity oscillations observed in this figure. When a bead is no longer in contact with its neighbors, it has, from equations (11) a constant velocity. Thus, before the end of the collision ($v_1 = const.$), the bead 7 separates from the column ($v_7 = const.$), then the sixth, the fifth, the fourth before the last three beads bounce together almost at the same time. Moreover, the beads of the top of the column, 7 to 4, separate from the column with a greater velocity than their initial one, whereas the beads at the bottom bounce upwards with a smaller velocity than their initial one. For instance, at the end of the collision, the velocity of the bead 7 is about 150% of its initial velocity (see Fig. 19).

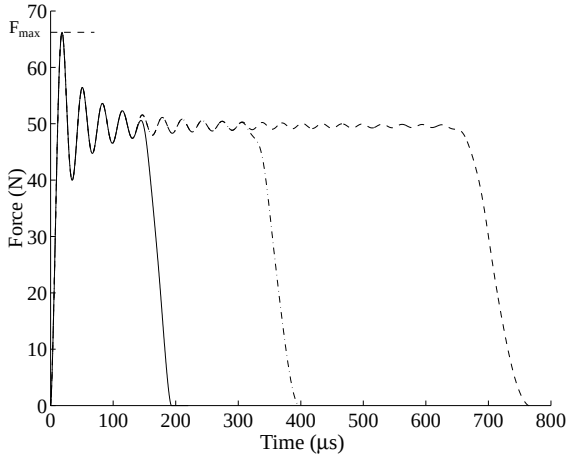

Fig. 20. Result of numerical simulations: temporal evolution of the force felt by the wall for a collision of $N = 7$ beads (solid line); $N = 15$ beads (dot-dashed line) or $N = 30$ beads (dashed line). The parameters of the simulation, N excepted, are as in Figure 18. F_{max} is the maximum force felt by the wall. This figure should be compared with the experimental results in Figure 4.

6.2 Force felt by the wall during the collision

Figure 20 shows the temporal evolution of the force F_0, felt by the wall, for a collision with $N = 7$, 15 or 30 beads. The force profile is in agreement with the experimental results for a rigid wall: the force increases till a value F_{max}, independent of N, then oscillates about a constant value with a period P independent of N. Those force oscillations are connected with the oscillating motion of the bead 1 (see Fig. 18). Unlike the experimental results, simulations show that the mean value of the force is constant during all the collision. This is due to the non–dissipative nature of the numerical model.

The maximum force $F_{max}(N)$ is independent of N, and equal to the maximum force $F_{max}(1)$ felt by the wall during the fall of one single bead. Consequently, we may assume that the expression of $F_{max}(N)$ is independent of the parameter k which is characteristic of a contact between two beads (see Eq. (12)). Using dimensional analysis, we obtain easily the expression of the maximum force

$$F_{max}(N) = N^0 F_{max}(1) = C_1 m^{3/5} v_{imp}^{6/5} K^{2/5} \ , \qquad (13)$$

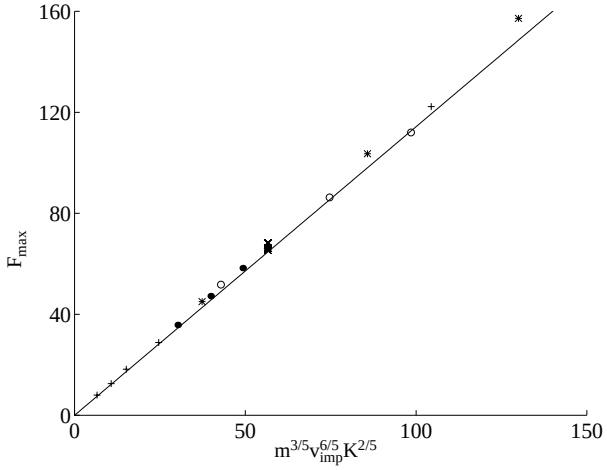

Fig. 21. Result of numerical simulations: maximum force F_{max}, in Newton, as a function of $m^{3/5}v_{imp}^{6/5}K^{2/5}$ for various values of the numerical parameters: N, k, K, m and v_{imp}; (+) correspond to $m = 2.05 \times 10^{-3}$ kg, $k = 6.9716 \times 10^9$ N/m$^{3/2}$ and $K = 9.858 \times 10^9$ N/m$^{3/2}$ when v_{imp} varies from 0.05, 0.075, 0.1, 0.15, 0.3 to 0.5 m/s. For each value of v_{imp}, F_{max} is identical when N varies from 3 to 10; (∗) correspond to $N = 8$, $v_{imp} = 0.3$ m/s, $k = 6.9716 \times 10^9$ N/m$^{3/2}$ and $K = 9.858 \times 10^9$ N/m$^{3/2}$ when m varies from 1.025×10^{-3}, 2.05×10^{-3}, 4.1×10^{-3} to 8.2×10^{-3} kg; (○) correspond to $N = 8$, $m = 2.05 \times 10^{-3}$ kg, $v_{imp} = 0.3$ m/s and $k = 6.9716 \times 10^9$ N/m$^{3/2}$ when K varies from 4.929×10^9, 9.858×10^9, 1.971×10^{10} to 2.957×10^{10} N/m$^{3/2}$; (×) correspond to $N = 8$, $m = 2.05 \times 10^{-3}$ kg, $v_{imp} = 0.3$ m/s and $K = 9.858 \times 10^9$ N/m$^{3/2}$ when k varies from 3.486×10^9, 6.9716×10^9, 1.394×10^{10} to 2.091×10^{10} N/m$^{3/2}$; (•) correspond to $N = 7$, $m = 2.05 \times 10^{-3}$ kg, $v_{imp} = 0.3$ m/s when $K = k$ varies from 2×10^9, 4×10^9, 6.9716×10^9 to 9.858×10^9 N/m$^{3/2}$. The solid line corresponds to $C_1 m^{3/5} v_{imp}^{6/5} K^{2/5}$ with $C_1 = 1.143$.

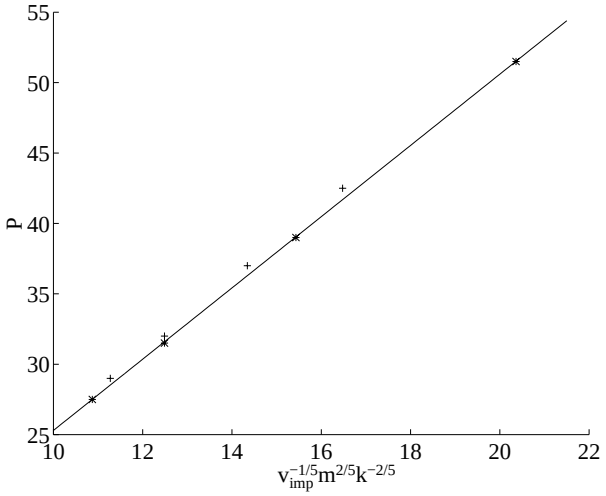

Fig. 22. Result of numerical simulations: period P, in μs, of the force oscillations as a function of $v_{imp}^{-1/5}m^{2/5}k^{-2/5}$ for various values of the numerical parameters: N, k, K, m and v_{imp}; (+) correspond to $m = 2.05 \times 10^{-3}$ kg, $k = 6.9716 \times 10^9$ N/m$^{3/2}$ and $K = 9.858 \times 10^9$ N/m$^{3/2}$ when v_{imp} varies from 0.075, 0.15, 0.3 to 0.5 m/s. For each value of v_{imp}, P is identical when N varies from 3 to 10; (∗) correspond to $N = 7$, $m = 2.05 \times 10^{-3}$ kg, $v_{imp} = 0.3$ m/s when $K = k$ varies from 2×10^9, 4×10^9, 6.9716×10^9 to 9.858×10^9 N/m$^{3/2}$. The solid line corresponds to $C_2 v_{imp}^{-1/5} m^{2/5} k^{-2/5}$ with $C_2 = 2.53$.

where K is defined in equation (3) and C_1 is a numerical constant. Figure 21 shows the values of $F_{max}(N)$ as a function of $m^{3/5}v_{imp}^{6/5}K^{2/5}$ when the numerical parameters (*i.e.*, N, k, K, m and v_{imp}) are varied. These numerical calculations confirm that F_{max} is independent of k (see (×) mark in Fig. 21). The slope of the solid line in Figure 21 corresponds to $C_1 = 1.143$. The expression of $F_{max}(1)$ derived from Hertz's theory reads [37]

$$F_{max}(1) = \left(\frac{5}{6}\right)^{2/5} \left[\frac{5m^3 v_{imp}^6 R}{\left(\frac{1-\nu_s^2}{E_s} + \frac{1-\nu_p^2}{E_p}\right)^2}\right]^{1/5} . \qquad (14)$$

Substituting equation (3) into equation (14), the theoretical value for C_1 is $(5/6)^{2/5}(45/16)^{1/5} \simeq 1.143$, in agreement with the simulation.

The numerical value of the maximum force in Figure 20 is found to be $F_{max}^{num} = 66.2$ N. This value is in fair agreement with the experimental's one $F_{max}^{exp} = 69$ N (see Sect. 3.1) and with the theoretical's one $F_{max}^{theo} = 65.3$ N calculated by equation (14) for $v_{imp} = 0.3$ m/s; $m = 2.05 \times 10^{-3}$ kg; $R = 4$ mm; $\nu_s = \nu_p = 0.276$ and $E_s = E_p = 21.6 \times 10^{10}$ N/m^2. The experimental value is slightly greater than the theoretical and numerical ones since the experimental impact velocity is slightly greater than 0.3 m/s.

6.3 Period of the force oscillations during the collision

The period P of the force oscillations in Figure 20 is independent of N. In this figure, the period of oscillations is $P = 31.5$ μs. This value is in fair agreement with the experimental result $P_{exp} = 31.2$ μs (see Sect. 3.1). If the interpretation of these force oscillations, given in Section 6.1, is valid, the period P must be independent of K. Then, using dimensional analysis, we easily obtain

$$P = C_2 \left(\frac{m}{k}\right)^{2/5} v_{imp}^{-1/5} , \qquad (15)$$

where C_2 is a numerical constant. The numerical simulations agree with equation (15) and consequently confirm the interpretation given in Section 6.1. Figure 22 shows the values of P as a function of $v_{imp}^{-1/5}m^{2/5}k^{-2/5}$ when the numerical parameters (*i.e.*, N, k, K, m and v_{imp}) are varied. The slope of the solid line corresponds to $C_2 = 2.53$.

6.4 Duration of impact of a column of N beads

The duration of impact τ_N is shown in Figure 23 as a function of N. τ_N is a linearly increasing function of N,

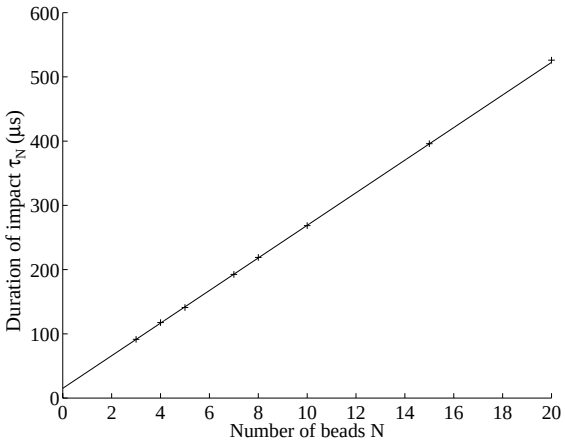

Fig. 23. Result of numerical simulations: duration of impact τ_N as a function of N. The parameters of the simulation, excepted N, are as in Figure 18. Crosses correspond to numerical points. The solid line corresponds to $\tau_N = (N-1)T_q + \tau_1$ with $T_q = 25.4$ μs and $\tau_1 = 40.6$ μs. This figure may be compared with the experimental results in Figure 7.

such that $\tau_N = (N-1)T_q + \tau_1$, where $T_q = 25.4$ μs is given by the slope of the solid line and $\tau_1 = 40.6$ μs from the intercept of the solid line and the vertical $N = 1$. The physical meaning of T_q has been explained in Section 3.3 (see also the next section). The numerical value of τ_1 is in agreement both with the value $\tau_1^{theo} = 34.2$ μs derived from Hertz's theory for a sphere–plane contact (see Eq. (2)) and with the experimental one $\tau_1^{exp} = 35.5$ μs (see Sect. 3.2).

Moreover, the evolution of τ_N is governed by the same equation as equation (4) found experimentally. However, this equation differs from the one obtained by Luding *et al.* [35,43] in molecular–dynamics simulations. Using a dissipative linear interaction law, they find that the duration of impact τ_N is proportional to the number of beads and to the duration of impact of one single bead τ_1; hence $\tau_N \propto N\tau_1$. Moreover, although the duration of impact for a sphere–sphere contact differs from a sphere–plane contact, the single sphere–plane contact occurring during the collision among all the sphere–sphere contacts does not imply that $\tau_N \neq N\tau_1$. Indeed, equation (4) is valid for simulations with a sensor represented by a plane with a stiffness $K \neq k$ as well as with a sensor represented by a portion of a sphere with a stiffness $K = k$. During these simulations, the value of τ_1 changes whereas the value of T_q is identical. This is in agreement with the interpretation of T_q given in Section 3.3.

6.5 Velocity of the deformation wave in the column

At the beginning of the impact of the column with the wall, a deformation wave is generated from the contact point. During the collision, this wave propagates upwards, then is reflected and comes back to where it started at the end of the collision, *i.e.*, when the column separates from the wall. At a fixed impact velocity and varying the number of beads, we find that the numerical results are consistent with the experimental ones (see Sect. 3.3) and the theoretical one (see Sect. 7): the velocity v of the deformation wave is independent of N, and v can be expressed as a ratio of the length to come and go in one bead to the time T_q to cover this distance, *i.e.*, $v = 4R/T_q$. For $v_{imp} = 0.3$ m/s, T_q is given by the slope of the solid line in Figure 23. Substituting this value into equation (6), R being equal to 4 mm for the calculation of k and K, the velocity then is $v = 630.7$ m/s. This value is in agreement with the slope $v = 630.5$ m/s of the solid line in Figure 24a for $v_{imp} = 0.3$ m/s.

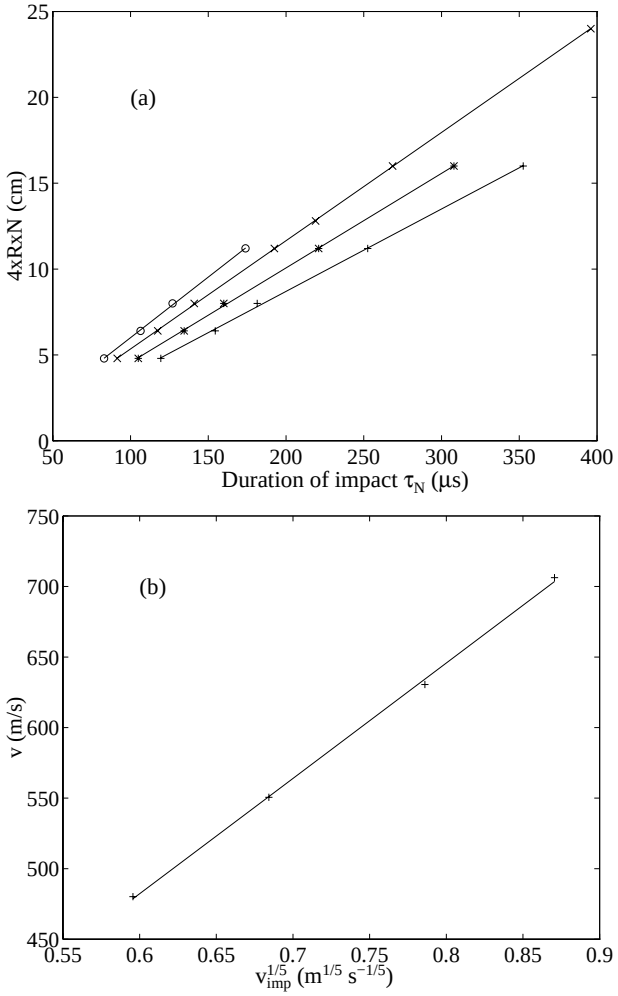

Fig. 24. Result of numerical simulations: (a) length covered by the deformation wave (*i.e.*, twice the length of the column $4 \times R \times N$) as a function of the time spent by the wave to cover this length (*i.e.*, the duration of impact) for different impact velocities v_{imp} of the column: (+) 0.075; (∗) 0.15; (×) 0.3 and (∘) 0.5 m/s. The slopes of the solid lines give the wave velocities $v = 480.2$; 550.6; 630.5 and 706.3 m/s for $v_{imp} = 0.075$; 0.15; 0.3 and 0.5 m/s respectively. (b) Velocity v of the deformation wave as a function of $v_{imp}^{1/5}$. In both cases, the parameters of the simulation, v_{imp} excepted, are as in Figure 18.

Figure 24a shows that, at a fixed impact velocity, the wave velocity is independent of the number of beads N. Plotting the wave velocity v as a function of the impact

velocity v_{imp}, as in Figure 24b, we see that v scales as $v_{imp}^{1/5}$. Thus, the faster the column hits the wall, the greater the velocity of the deformation wave. In Table 1, the numerical results are compared to the experimental ones for three different values of impact velocity $v_{imp} = 0.191$; 0.246 and 0.316 m/s corresponding respectively to three heights of fall $h = 1.9$; 3.1 and 5.1 mm.

The interpretation of T_q in Section 3.3 implies that it is independent of K. Thus, from equation (6), the velocity v is also independent of K. Using these assumption and a dimensional argument, we obtain easily

$$v = C_3 \left(\frac{k}{m}\right)^{2/5} R v_{imp}^{1/5} , \qquad (16)$$

where C_3 is a numerical constant. When the numerical parameters k, m and v_{imp} are varied, we found numerically the constant $C_3 = 2$. Substituting equation (16) into equation (6), T_q has the following expression

$$T_q = C_3 \left(\frac{m}{k}\right)^{2/5} v_{imp}^{-1/5} . \qquad (17)$$

6.6 Detachment of the beads from the column

At the end of the collision, knowing the individual motion of each bead, we are able to decide whether the column bounces as a whole, or whether the beads separate one after the other from the column. We define the end of the column–wall collision as the time at which the bead at the bottom leaves the wall ($x_1 < 0$). For a column of N beads, the distribution of velocities of each bead, at the end of the collision, is the set of values $|\dot{x}_i(t = \tau_N)|$ for $i = 1, \ldots, N$. Figure 25 shows the velocity distribution for different values of N. Two sorts of velocity distributions appear distinctly in this figure: the upper beads of the column go away with velocities greater than v_{imp} while the lower beads have velocities smaller than v_{imp}. For instance, for a column of $N = 7$ beads, the bead 7 go away with 150% of its initial velocity whereas the bead 1 disposes only of 30% of its initial velocity. We will see below that those two sorts of velocity distributions correspond to two sorts of beads separation. Moreover, considering only the upper beads with velocities greater than v_{imp}, Figure 25 shows that these beads have a velocity which tends asymptotically to v_{imp} when N decreases.

Let us define the time of detachment of the ith bead as the time, from the beginning of the impact, where the ith bead separates from the $i+1$th one or from the $i-1$th one. The times of detachment of the N beads of the column are plotted in Figure 26 for various values of N. For $N < 5$, the beads separate one after the other from the top of the column. For $N \geq 5$, two regimes arise: the beads of the top separate one after the other from the top of the column, as in the previous case, till the beads at the bottom bounce upwards as a whole (*i.e.*, till the first bead leaves the wall taking the remaining beads off with it).

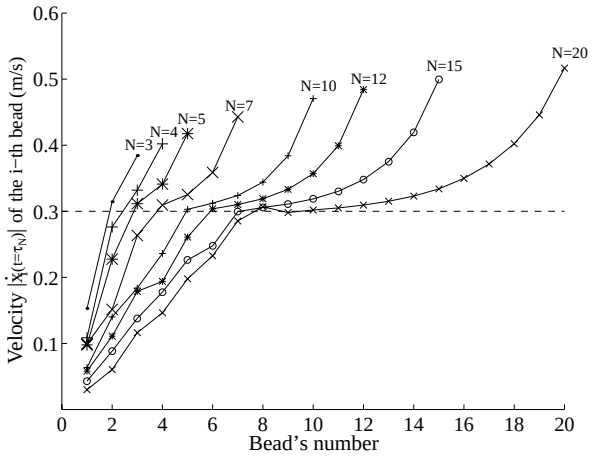

Fig. 25. Result of numerical simulations: velocity of the ith bead, at the end of the collision, as a function of the bead's number i, for different values of N: (·) 3; (+) 4; (∗) 5; (×) 7; (+) 10; (∗) 12; (○) 15; (×) 20. For all curves, the parameters of the simulation are as in Figure 18.

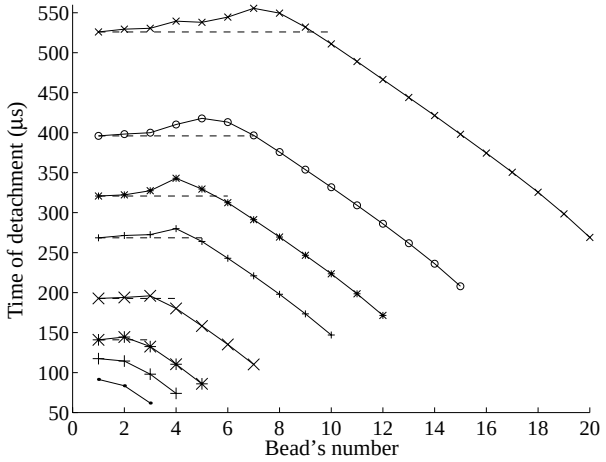

Fig. 26. Result of numerical simulations: time of detachment of the ith bead as a function of the bead's number i, for various values of N: (·) 3; (+) 4; (∗) 5; (×) 7; (+) 10; (∗) 12; (○) 15; (×) 20. For each value of $N \geq 5$, each dashed line corresponds to the time beyond which the beads at the bottom of the column bounce upwards as a cluster (*i.e.*, when the first bead leaves the wall taking the remaining beads with it). For all curves, the parameters of the simulation are as in Figure 18.

The beads in the cluster that leaves the wall, still interact with each other, after the end of the collision, and separate from each other starting, this time, by the lower bead (see Fig. 26). If we compare Figures 25 and 26, we note that the upper beads which separate one after the other, are the beads which go away with velocities greater than the initial ones whereas the beads at the bottom which separate as a whole, correspond to the beads which have lower velocities than v_{imp}.

Let us now define the number of beads N_s which separate one after the other from the column. The $N - N_s$ other ones then are the number of beads in the cluster. For each value of N, N_s is given by the number of data

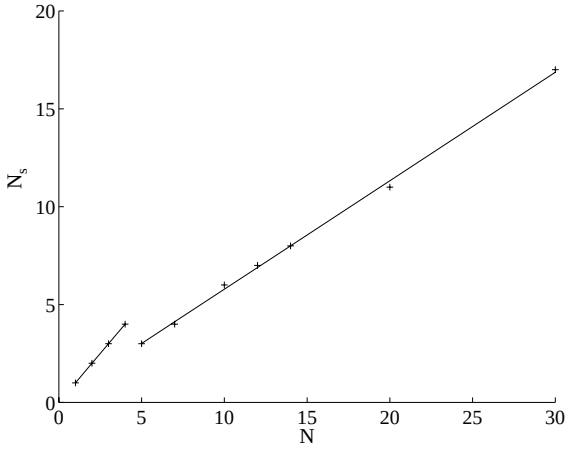

Fig. 27. Result of numerical simulations: evolution of N_s as a function of N. For $N < 5$, the solid line corresponds to $N_s = N$ whereas for $N \geq 5$, the linear fit leads to a slope of 0.55.

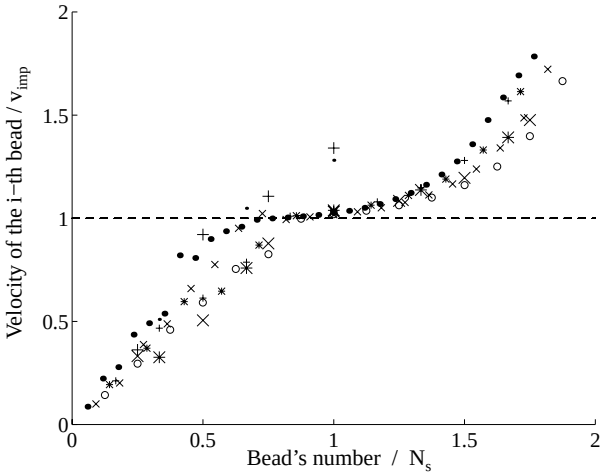

Fig. 28. Result of numerical simulations: velocity of the ith bead, at the end of the collision, divided by the impact velocity v_{imp} as a function of the bead's number i divided by N_s, for different values of N. All symbols used are as in Figure 25 except for $N = 30$ (•). The results of Figure 25 all lie on the same curve except for $N = 3$ (·) and 4 (┼). Beads with final velocities greater then their initial ones v_{imp} are above the dashed–line whereas beads with final velocities smaller than v_{imp} are below this dashed–line.

being below each dashed–line in Figure 26. Figure 27 shows the evolution of N_s as a function of N. As it has been noticed above, for $N < 5$, $N_s = N$. For $N \geq 5$, N_s is well described by a linear fit with a slope greater than 1/2. This means that for a fixed value of N, the number of beads which separate one after the other from the column is always greater than the one in the cluster. To look for the scaling behavior of both the velocities distribution at the end of the collision in Figure 25 and the times of detachment distribution in Figure 26, we rescale the abscissa–axis in both figures by N_s. The ordinate–axis in Figure 25 is nondimensionalized with the impact velocity v_{imp} and the one in Figure 26 with the duration of the impact τ_N. The results are shown in Figures 28 and 29. Both figures show that all results (except data for $N < 5$) lie on a single curve.

Since the total energy is conserved in our model, the energy of the system is redistributed during the collision, leading to the bead detachment effect. As shown by Figure 30 for a collision of a column of $N = 5$ beads, the interaction forces between the upper beads are stronger, but occur over a shorter time interval, than between the lower beads of the column. The energy redistribution occurs during the interactions between the beads, mostly from the regions where the interactions are weak but occur over a long time interval to the regions where the interactions are strong but occur over a small time interval.

The kinetic energy of the column is defined, relatively to its center of mass, as

$$E_{rel}(t) = \frac{m}{2} \sum_{i=1}^{N} (\dot{x}_i(t) - v_g)^2 \ , \qquad (18)$$

where v_g is the velocity of the center of mass of the column, defined as

$$v_g = \frac{1}{N} \sum_{i=1}^{N} \dot{x}_i(t) \ . \qquad (19)$$

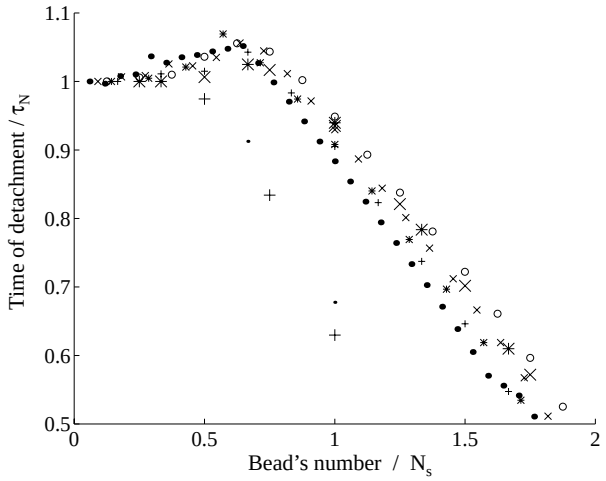

Fig. 29. Result of numerical simulations: time of detachment of the ith bead divided by the duration of impact τ_N as a function of the bead's number i divided by N_s, for various values of N. All symbols used are as in Figure 26 except for $N = 30$ (•). The results of Figure 26 all lie on the same curve except for $N = 3$ (·) and 4 (┼).

E_{rel} is also called *granular temperature* when $N \gg 1$. At the end of the collision ($t = \tau_N$), E_{rel} gives a measure of the typical separation of the beads, since the contributions in the sum in equation (18) are significant only for $\dot{x}_i \gg v_g$ or $\dot{x}_i \ll v_g$. Previously, we have established that the greater the number of beads N, the greater the excess velocity of the upper beads from their initial velocity, v_{imp}. Thus, E_{rel} must increase with N. However, when

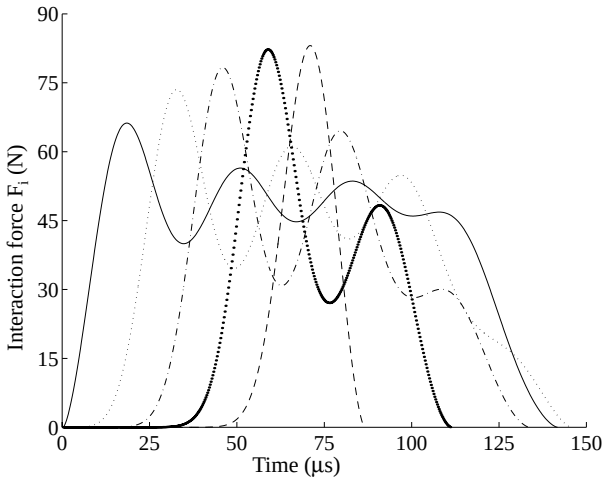

Fig. 30. Result of numerical simulations: interaction force F_i between the ith and the $i+1$th bead as a function of time, during the collision of a column of $N = 5$ beads and the wall: $(-)$ F_0 bead 1 with a wall; $(\cdot)$ F_1 beads 1 and 2; $(-\cdot)$ F_2 beads 2 and 3; $(\bullet)$ F_3 beads 3 and 4; $(--)$ F_4 beads 4 and 5. For all curves, the parameters of the simulation are as in Figure 18.

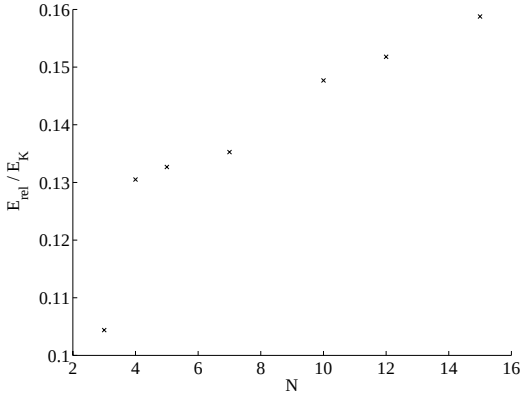

Fig. 31. Result of numerical simulations: evolution of E_{rel}/E_K as a function of the number of beads N. Crosses are the numerical points. For all numerical points, the parameters of the simulation are as in Figure 18.

the number of beads N increases, so does the total energy of the system. The interesting quantity is then the ratio of the relative kinetic energy E_{rel} at the end of the collision, to the total kinetic energy E_K, *i.e.*,

$$\frac{E_{rel}}{E_K} = \frac{\sum_{i=1}^{N} (\dot{x}_i\big|_{t=\tau_N} - v_g\big|_{t=\tau_N})^2}{\sum_{i=1}^{N} \dot{x}_i^2\big|_{t=\tau_N}} \cdot \qquad (20)$$

The evolution of this ratio is represented in Figure 31 as a function of N. At the end of the collision, the typical separation between each bead increases with N. Obviously, this result is no longer valid in the case of a dissipative model, with a linear interaction law, since the typical separation passes through a maximum, at a small value of N, then decreases at higher values of N (see Fig. 2c in Ref. [35]).

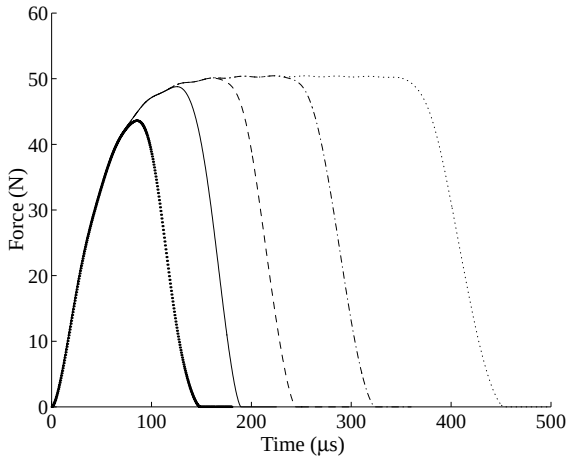

Fig. 32. Result of numerical simulations: temporal evolution of the force felt by a soft wall for a collision of $N = 3$ $(\bullet)$; 5 $(-)$; 7 $(--)$; 10 $(-\cdot)$ and 15 $(\cdot)$ beads.

6.7 Collision with a soft wall

Let us now consider the case of a collision with a soft wall. Such a collision have been defined in Section 3.3 when $\tau_{max}(N = 1) \geq T_q$ whereas a collision with a rigid wall correspond to $\tau_{max}(N = 1) < T_q$. Since dissipation is not taken into account, the maximum force of the loading cycle of a single bead, *i.e.*, $N = 1$, is reached at half the duration of a collision, *i.e.*, when

$$\tau_{max}(N = 1) = \frac{\tau_1}{2} \cdot \qquad (21)$$

The substitution of equations (2), (17) and (21) into the two above inequations then leads to a critical coefficient K_c of the sphere–plane contact,

$$K_c = \left(\frac{2.94}{4}\right)^{5/2} \frac{5k}{4} \, , \qquad (22)$$

such that for $K > K_c$ the collision is defined as a rigid wall collision and for $K \leq K_c$ as a soft wall one.

In almost all simulations of Section 6, the value of the Hertz's coefficient for a sphere–sphere contact is the one between two stainless steel spheres, *i.e.*, $k = 6.9716 \times 10^9$ N/m$^{3/2}$. Consequently, with equation (22) and for a column of stainless steel spheres, the critical value is $K_c = 4{\times}10^9$ N/m$^{3/2}$. In Section 6.2, we have shown that the evolution of the maximum force F_{max}, felt by the wall, is independent of N. This behavior is consistent with the above remarks since the value of the parameter $K = 9.858 \times 10^9$ N/m$^{3/2}$ was such that $K > K_c$. Figure 32 shows the temporal evolution of the force F_0 for a collision with $N = 3$, 5, 7, 10 or 15 beads with $K < K_c$. The parameters of the

simulations are $K = 1 \times 10^9$ N/m$^{3/2}$; $k = 6.9716 \times 10^9$ N/m$^{3/2}$; $v_{imp} = 0.3$ m/s and $m = 2.05 \times 10^{-3}$ kg. As expected, the force profile is in agreement with the experimental results for a soft wall: the force increases till a value F_{max} which depends on N, at low values of N, and is independent of N at higher values. Unlike the experimental results (see for example Fig. 13d), simulations in Figure 32 show that the mean value of the force is constant during all the collision. This results of the absence of dissipative effects in the numerical simulation.

7 Analytical expression of the velocity of the deformation wave

In the absence of gravity, it is equivalent to consider a column of beads of velocity v_{imp} bouncing on a wall or a column which would be pushed away by a wall moving at constant velocity $v_w = -v_{imp}$. The analytical expression of the velocity v of the deformation wave can be derived in analogy with the derivation of the velocity of longitudinal waves in a uniform bar of semi-infinite length, subjected to a force step[6]. At $t = 0$, consider a compression force suddenly applied to a end of the chain of beads in contact, each with a radius R. A compression wave begins to propagate through the chain with velocity v. After a time $t > 0$, the wave has covered a distance $L = vt$ while the application point of the force has covered a distance $\Delta L = v_{imp}t$. The number N_f of beads in motion, at time t, is[7]

$$N_f = \frac{vt}{2R} \cdot \tag{23}$$

The conservation of momentum, at the same instant, implies

$$Ft = N_f m v_{imp} \ , \tag{24}$$

m being the mass of one bead. The Hertz interaction law links the interpenetration δ of two beads to the force F which compress them one to another, as [37]

$$\delta = \left(\frac{F}{k}\right)^{2/3} \ , \tag{25}$$

where k is the coefficient of the Hertz's law for a sphere–sphere contact (see Eq. (12)). At time t, the application point of the force will have covered a length[8] $\Delta L = N_f\delta =$ $v_{imp}t$. Substituting equation (25) into the expression of ΔL, we find

$$\frac{vt}{2R}\left(\frac{F}{k}\right)^{2/3} = v_{imp}t \ . \tag{26}$$

Eliminating F from equations (24) and (26), and using equation (23), the velocity v of the deformation wave through the beads chain is then

$$v = 2\left(\frac{k}{m}\right)^{2/5} R v_{imp}^{1/5} \ . \tag{27}$$

This equation has the same expression as equation (16) found numerically, with the same numerical coefficient.

Moreover, in contrast with the homogeneous bar case, the interaction between the beads is nonlinear. As a consequence, the velocity of the deformation wave depends on the impact velocity v_{imp} in the nonlinear case whereas sound velocity in a bar is independent of v_{imp}.

Besides, we note that equation (27) can be linked to the velocity of a soliton: in a horizontal chain of beads, if the initial impact velocity, at one side of the chain, is great ($v_{imp} = 5$ m/s), Nesterenko and Lazaridi [21,22] show numerically that it is possible to propagate a soliton, through the chain of beads, with a typical size of the order of 5 beads and with a front velocity v_{sol} smaller than the velocity v of the deformation wave

$$v_{sol} = \left(\frac{4}{5}\right)^{2/5} v \ . \tag{28}$$

Substituting equation (27) into equation (6), the time T_q spent for the transfer of momentum from one bead to another is then

$$T_q = 2\left(\frac{m}{k}\right)^{2/5} v_{imp}^{-1/5} \ . \tag{29}$$

This equation has the same expression as equation (17) found numerically, with the same numerical coefficient. With $E_s = 21.6 \times 10^{10}$ N/m^2; $\nu_s = 0.276$; $\rho_s = 7850$ kg/m^3; and using equations (12), (27) and $m = 4\pi R^3\rho_s/3$, the velocity of the deformation wave is calculated for three different values of impact velocity $v_{imp} = 0.191$; 0.246 and 0.316 m/s corresponding respectively to three heights of fall $h = 1.9$; 3.1 and 5.1 mm. These results are listed in Table 1 and are in agreement both with the velocities measured experimentally in Section 3.3 and the ones deduced from the simulation in Section 6.5.

8 Mechanism of the bead detachment effect

Consider now a one–dimensional column of N identical beads, all at a distance d_0 apart and having an initial velocity $v_i^{\mathrm{i}} = v_{imp}$ along their common axis. Neglecting the gravity effects, let this column hit a static wall. After the collision, the beads move away from the wall with a velocity v_i^{f}. Luding *et al.* [35,43,45] have studied this

[6] This elementary derivation of the formula for the velocity of longitudinal waves in uniform bars is originally due to Babinet; see reference [44].

[7] In practice, as a chain of beads is dispersive (see Sect. 8), the front of the deformation wave changes of shape while propagating through the chain. Equation (23) is thus only approximate.

[8] Actually, there are $N_f - 1$ contacts and thus $\Delta L = (N_f - 1)\delta$, but we assume $N_f \gg 1$.

problem (see also Ref. [46] for a brief description), with molecular–dynamics simulations, using a dissipative linear or nonlinear interaction law between beads in contact. They have measured the effective restitution coefficient ϵ_{col} of the whole column defined as

$$\epsilon_{col} \equiv \sqrt{\frac{\sum_{i=1}^{N} v_i^{\mathrm{f}\,2}}{\sum_{i=1}^{N} v_i^{\mathrm{i}\,2}}} = \frac{1}{N v_{imp}} \sqrt{\sum_{i=1}^{N} v_i^{\mathrm{f}\,2}} \,. \qquad (30)$$

They have shown that ϵ_{col} depends on the ratio t_0/τ_N, where $t_0 = d_0/v_{imp}$ is the time needed for a bead to catch up with the bead in front of it when the latter is suddenly stopped (*e.g.*, by impact on a wall) and τ_N the duration of collision of the whole column. In the limiting case $t_0/\tau_N \gg 1/N$, the collision between the column and the wall leads to a large number of binary collisions between beads. The effective restitution coefficient ϵ_{col} is thus considerably smaller than the coefficient of restitution for a binary impact. On the other hand, in the limiting case $t_0/\tau_N \ll 1/N$, the collision between the column and the wall leads to all beads in mutual contact at the same time. Thus, the beads interact with the wall as a chain of coupled damped oscillators rather than as N distinct beads. The effective restitution coefficient ϵ_{col} is close to one in this case, and the beads separates from each other with large fluctuations in the interbead distances: this behavior was called the *detachment effect* [35], but has no clear interpretation.

In our problem $d_0 = 0$ since all beads are in mutual contact during the free fall of the column, and we find again the detachment effect predicted by Luding *et al.* We have shown experimentally in Section 3.5, although in an indirect way, that the beads are no longer in contact after the collision. Besides, we have shown numerically in Sections 6.1 and 6.6, that after the compressive cycle, two sorts of detachment effects arise according to whether the number of beads in the column is greater or smaller than a critical number. In both cases, the beads separate from each other with large fluctuations in the interbead separations (see Fig. 18) and with large fluctuations in velocities (see Figs. 19 and 25).

The detachment effect is essentially due to the elastic properties of the beads material since simulations [35] for $d_0 = 0$, in the limit of very hard interaction (*i.e.*, the duration of impact is zero), shows that this effect almost vanishes (*i.e.*, the separation between each bead is constant and very small compared to soft–sphere interaction, see Figs. 1a and 1d in Ref. [35]). Moreover, for a dissipative linear model and $d_0 = 0$, Luding *et al.* showed that the detachment effect is the result of model–dependent dissipative properties [35]. Indeed, it seems reasonable that a column of steel beads have to disperse more than a column of aluminium beads (the collision of the whole column of steel beads is less dissipative than the aluminium one) since a binary collision between steel beads is weakly dissipative whereas the one between aluminium beads is strongly dissipative. However, the dissipation is not the cause of this effect since the Hertz nonlinear interaction model, presented in Sections 5 and 6, which is non–dissipative, exhibits the bead detachment effect from the column.

The cause of this detachment effect is the redistribution of energy within the whole system during the collision. This redistribution takes place because the energy propagation through the column of beads is dispersive (see also Ref. [17]).

To understand this, consider now the case of an horizontal chain of N identical elastic beads, each one suspended by two threads, which is hit by n incident beads. During the collision, the incident energy of impacting beads is distributed through the whole chain, this latter being slightly dispersive. The energy and momentum transfers are called dispersive because, at the end of the collision, each bead has a fraction of the incident energy. Thus, at the end of the collision, the $N-n$ beads, usually looked upon as being motionless and in mutual contact (see Sect. 1), are in motion and are separated from their neighbors by a small distance. On the contrary, a system exhibits *dispersion–free* [32] or *perfect* transmission [33] if the perturbation generated during the impact propagates through the chain without changing its shape and, then, transfers its momentum and energy to the n beads at the far end of the chain. Such systems are made of different beads, with different masses interacting through springs of different stiffness, either linear or nonlinear [32,33]. For linear interaction (Hooke's law), Reinsch [33] found analytically the mass of each beads and the stiffness of each spring for perfect transmission whatever N and n. In the continuum limit, this perfect transmission chain is related to a dispersion–free wave equation. For nonlinear interaction (Hertz's law), numerical simulations for $N = 3$, $n = 1$ [33] and $N = 4$, $n = 1$ [32] show that, for indentical beads, the chain is dispersive. However, for Hertz's interaction and different beads, perfect transmission chain may be obtained [33]. In the well-known commercial experiment with $n = 1$ and $N \simeq 5$ identical beads, after the first collision, one single bead moves away at the far end, the others being now separated from their neighbors by small distances. In the following collisions, the chain is a dispersion–free system since only binary collisions occur. This interpretation is originally due to Herrmann *et al.* [32].

Let us now return to our problem, neglecting dissipative effects. It is the same problem as above with $n = 1$, N identical elastic beads and realistic interaction between them, *i.e.*, Hertz's law. Therefore, the perfect transmission of the column (*i.e.*, no bead detachment effect) cannot rise, whatever the value of N. Moreover, Luding *et al.* [35,43,45] have noted that the detachment effect is weaker for nonlinear interactions (Hertz's law) than for linear interactions (Hooke's law). This is reasonable since a chain of identical beads with Hertz's interaction is, by nature, less dispersive than the one with Hooke's interaction [32,33]. Thus, it seems normal that in the limit of hard spheres, *i.e.*, strongly nonlinear interactions, the detachment effect nearly vanishes, since the system becomes

non–dispersive. During the collision of a column of beads with a wall, the slight energy dispersion is responsible for the energy redistribution within the whole column and therefore for the bead detachment effect. Consequently, this mechanism is essentially non–dissipative, but obviously may be dependent on dissipation in a realistic column.

9 Conclusion

An experimental study of the collision of a column of N beads with a fixed wall has been presented. For a fixed height of fall and a rigid wall, we have shown that the maximum force felt by the wall do not depend on the number of beads. We have also measured the duration of impact, the velocity of the deformation wave in the column and an effective restitution coefficient of the column as functions of N. Besides, we have emphasized that the independence of the maximum force on N is linked to the propagation of the deformation wave through the column and depends on the rigidity of the wall. Moreover, we are able to give a quantitative definition for this notion of *rigidity*. An analytical expression of the velocity of the deformation wave has been derived and is consistent with the experimental results.

A non-dissipative numerical model, based on the Hertz's interaction, gives results in fair agreement with the experiments. Moreover, we have shown numerically that, after the compression phase between the column and the wall, the beads separate from each other with large fluctuations in velocity and in the interbead distances. Two sorts of such bead detachment effect have been observed numerically: one below the critical number of beads $N = 5$ and one for $N \geq 5$. For $N \geq 5$, the beads at the top of the column separate one after the other from the column with a velocity greater than their initial one. The beads at the bottom then bounce upwards as a whole, with a velocity smaller than their initial one.

An interpretation of the bead detachment effect has been given. We have emphasized that this bead detachment effect results from the energy redistribution within the system during the collision, not from any dissipative effects. This redistribution takes place because of the energy propagation through the column of beads is dispersive.

Our work also shows that the collision of N inelastic beads with a fixed wall (*i.e.*, no energy source during the collision) is governed by two basic mechanisms: the energy dispersion through the whole column and the energy dissipation due to the inelastic collision. The role of the energy dispersion is to redistribute the energy through the whole system during the collisions. This redistribution depends essentially on the intrinsic nature of the interaction law between two beads (*i.e.*, the Hertz's law for realistic interactions). The energy dispersion through the system then leads to the bead detachment effect from the column and to a typical separation between each bead. We have seen numerically that this typical separation increases with N. On the other hand, since some energy is lost during the collision, the dissipation tends to reduce this typical separation between each beads. The dissipation and the dispersion are thus antagonistic effects. Moreover, the dissipated energy increases with N (see Fig. 11). Therefore, if the dissipative effects balance the dispersive ones, *i.e.*, when N is very large, we think that the column will not bounce.

Finally, these mechanisms are not specific to one–dimensional experiments and must be very important for more realistic experiments in two or three dimensions: the purely dispersive effect (*i.e.*, the bead detachment effect) is probably a precursor mechanism for the fluidization of the vibrated granular media [9,10] whereas the preponderance of the dissipative effects may result to the condensed (or clustered) phase of the vibrated granular media [10,35].

We thank S. Luding for sending us his simulations of ϵ_{eff} which are taken from reference [42]. We gratefully acknowledge financial support from the MENESR trough the french laboratories network GEO and from the CNES through contrat 96/0318.

References

1. H.M. Jaeger, S.R. Nagel, R.P. Behringer, Phys. Today **49**, 32 (1996).
2. H.M. Jaeger, S.R. Nagel, Science **255**, 1523 (1992).
3. T. Travers, D. Bideau, A. Gervois, J.P. Troadec, J.C. Messager, J. Phys. A **19**, L1033 (1986).
4. J.P. Bouchaud, M. Cates, P. Claudin, J. Phys. France **5**, 639 (1995).
5. C. Laroche, S. Douady, S. Fauve, J. Phys. France **50**, 699 (1989).
6. J.B. Knight, E.E. Ehrichs, V.Y. Kuperman, J.K. Flint, H.M. Jaeger, S.R. Nagel, Phys. Rev. E **54**, 5726 (1996), and references therein.
7. P.K. Haff, J. Fluid Mech. **134**, 401 (1983).
8. S. Luding, E. Clément, A. Blumen, J. Rajchenbach, J. Duran, Phys. Rev. E **49**, 1634 (1994).
9. S. Warr, J.M. Huntley, G.T.H. Jacques, Phys. Rev. E **5**, 5583 (1995), and references therein.
10. A. Goldshtein, M. Shapiro, L. Moldavsky, M. Fichman, J. Fluid Mech. **287**, 349 (1995).
11. S. Fauve, S. Douady, C. Laroche, J. Phys. Colloq. France **50**, C3-187 (1989).
12. G.B. Lubkin, Phys. Today **48**, 17 (1995).
13. P.B. Umbanhowar, F. Melo, H.L. Swinney, Nature **382**, 793 (1996), and references therein.
14. R.S. Sinkovits, S. Sen, Phys. Rev. Lett. **74**, 2686 (1995).
15. J.D. Goddard, Proc. R. Soc. London, Ser. A **430**, 105 (1990).
16. C.-H. Liu, S.R. Nagel, Phys. Rev. Lett. **68**, 2301 (1992).
17. M.H. Sadd, Q. Tai, A. Shukla, Int. J. Non–Linear Mech. **28**, 251 (1993).
18. A. Shukla, C. Damania, J. Expt. Mech. **27**, 268 (1987).
19. C. Coste, E. Falcon, S. Fauve, in *Des géomatériaux aux ouvrages : expérimentations et modélisations*, in French, edited by C. Petit, G. Pijaudier–Cabot, J.-M. Reynouard (Hermes, Paris, 1995), p. 33-52.
20. C. Coste, E. Falcon, S. Fauve, Phys. Rev. E **56**, 6104 (1997).

21. A.N. Lazaridi, V.F. Nesterenko, J. Appl. Mech. Tech. Phys. **3**, 405 (1985).
22. V.F. Nesterenko, J. Appl. Mech. Tech. Phys. **5**, 733 (1983).
23. E. Falcon, C. Laroche, S. Fauve, C. Coste, Eur. Phys. J. B **3**, 45 (1998).
24. A.D. Bernstein, Am. J. Phys. **45**, 41 (1977).
25. P. Pieransky, J. Phys. France **44**, 573 (1983).
26. N.B. Tufillaro, T.M. Mello, Y.M. Choi, A.M. Albano, J. Phys. France **47**, 1477 (1986), and references therein.
27. W.R. Mellen, Am. J. Phys. **36**, 845 (1968).
28. W.G. Harter, Am. J. Phys. **39**, 656 (1971).
29. J.L. Spradley, Am. J. Phys. **55**, 183 (1987).
30. J. Walker, Sci. Am. **259**, 116 (1988).
31. F. Herrmann, P. Schmälzle, Am. J. Phys. **49**, 761 (1981).
32. F. Herrmann, M. Seitz, Am. J. Phys. **50**, 977 (1982).
33. M. Reinsch, Am. J. Phys. **62**, 271 (1994).
34. E.B. Kremer, A.Y. Fidlin, Sov. Phys. Dokl. **34**, 1063 (1989).
35. S. Luding, E. Clément, A. Blumen, J. Rajchenbach, J. Duran, Phys. Rev. E **50**, 4113 (1994).
36. B. Bernu, R. Mazighi, J. Phys. A **23**, 5745 (1990).
37. L.D. Landau, E.M. Lifshitz, *Theory of Elasticity*, 3rd ed. (Pergamon Press, Oxford, 1986).
38. S.C. Hunter, J. Mech. Phys. Solids **5**, 162 (1957).
39. J.P.A. Tillett, Proc. Phys. Soc. London, Sect. B **67**, 677 (1954).
40. J. Reed, J. Phys. D **18**, 2329 (1985).
41. O.R. Walton, in *Particulate two–phase flow*, edited by M.C. Roco (Butterworth–Heinemann, Boston, 1993), pp. 884–911.
42. S. Luding, Private communication, unpublished.
43. S. Luding, Ph.D. thesis, Universität Freiburg, 1994.
44. S.P. Timoshenko, J.N. Goodier, in *Theory of Elasticity*, 3rd ed. (McGraw–Hill, Singapore, 1970), pp. 493–494.
45. S. Luding, E. Clément, A. Blumen, J. Rajchenbach, J. Duran, in *Fractal aspects of materials*, edited by F. Family, P. Meakin, B. Sapoval, R. Wool (Materials Research Society, Symposium Proceedings, Pittsburgh, Pennsylvania, 1995), Vol. **367**, pp. 495–500.
46. J. Schäfer, S. Dippel, D.E. Wolf, J. Phys. I France **6**, 5 (1996).